**A THESIS SUBMITTED TO**
**THE GRADUATE SCHOOL OF NATURAL AND APPLIED SCIENCES**
**OF ÇANKIRI KARATEKİN UNIVERSITY**

# STRUCTURAL, PHYSICAL, AND MECHANICAL PROPERTIES OF THE (Cu-NANO MgO) SYSTEM BY POWDER METALLURGY METHOD

**IN PARTIAL FULFILLMENT OF THE REQUIREMENTS**
**FOR**
**THE DEGREE OF MASTER OF SCIENCE**
**IN**
**PHYSICS**

**BY**

**NOOR JASIM ZABOON AL-SAEDI**

**ÇANKIRI**

**2023**

STRUCTURAL, PHYSICAL, AND MECHANICAL PROPERTIES OF THE (Cu-NANO MgO) SYSTEM BY POWDER METALLURGY METHOD

By Noor Jasim Zaboon AL-SAEDI

February 2023

We certify that we have read this thesis and that in our opinion it is fully adequate, in scope and in quality, as a thesis for the degree of Master of Science

**Advisor** **:** Prof. Dr. Sebahaddin ALPTEKİN
**Co-Advisor** **:** Asst. Prof. Dr. Salih Younis DARWEESH

**Examining Committee Members:**

**Chairman** **:** Prof. Dr. Şemsettin ALTINDAL
Physics
Gazi University

**Member** **:** Prof. Dr. Sebahaddin ALPTEKİN
Physics
Çankırı Karatekin University

**Member** **:** Prof. Dr. Çiğdem YÜKSEKTEPE ATAOL
Physics
Çankırı Karatekin University

**Approved for the Graduate School of Natural and Applied Sciences**

**Prof. Dr. İbrahim ÇİFTÇİ**
**Director of Graduate School**

**I hereby declare that all information in this document has been obtained and presented in accordance with academic rules and ethical conduct. I also declare that, as required by these rules and conduct, I have fully cited and referenced all material and results that are not original to this work.**

**Noor Jasim Zaboon AL-SAEDI**

**ABSTRACT**

# STRUCTURAL, PHYSICAL, AND MECHANICAL PROPERTIES OF THE (Cu-NANO MgO) SYSTEM BY POWDER METALLURGY METHOD

Noor Jasim Zaboon AL-SAEDI

Master of Science in Physics

Advisor: Prof. Dr. Sebahaddin ALPTEKİN

Co-Advisor: Asst. Prof. Dr. Salih Younis DARWEESH

February 2023

The aim of this study was to prepare copper and MgO composites using powder metallurgy technique and to test the effect of nano MgO content on the structural, physical and mechanical properties of the composites. MgO was annealed in different percentages (2, 4, 6, 8, 10)% with copper percentages (98, 96, 94, 92, 90)%. The powders used were dried at 200 °C for one hour and after grinding and mixing for 2 hours, the samples were pressed and then thermally sintered in an oven at 900 °C for two hours. The results of the present study showed that copper can be strengthened using magnesium nanoparticles. Cu is a material that softens at high temperatures. By adding MgO to copper, it was observed that the material showed a different property and its hardness increased. Necessary tests such as apparent density, apparent density, microstructure, Vickers hardness, absolute porosity, EDS, water absorption, thermal conductivity, compressive strength and wear rate were performed. In addition, SEM (Scanning Electron Microscope) and XRD (X-Ray Diffraction) analyses were performed to find the structure of the material used.

**2023, 75 pages**

**Keywords:** Physical and mechanical properties, Powder metallurgy method

# ÖZET

## TOZ METALÜRJİSİ YÖNTEMİYLE (Cu-NANO MgO) SİSTEMİNİN YAPISAL, FİZİKSEL VE MEKANİK ÖZELLİKLERİ

Noor Jasim Zaboon AL-SAEDI
Fizik, Yüksek Lisans
Tez Danışmanı: Prof. Dr. Sebahaddin ALPTEKİN
Eş Danışman: Dr. Öğr. Üyesi Salih Younis DARWEESH
Şubat 2023

Bu çalışmada, toz metalurjisi tekniği kullanılarak bakır ve MgO kompozitlerinin hazırlanması ve nano MgO içeriğinin kompozitlerin yapısal, fiziksel ve mekanik özellikleri üzerindeki etkisinin test edilmesi amaçlanmıştır. MgO farklı yüzdelerde % (2, 4, 6, 8, 10) bakır yüzdeleri % (98, 96, 94, 92, 90) ile tavlanmıştır. Kullanılan tozlar bir saat boyunca 200 °C sıcaklıkta kurutulmuş ve 2 saat boyunca öğütülüp karıştırıldıktan sonra numuneler preslenmiş ve ardından iki saat boyunca 900 °C sıcaklıktaki bir fırında termal olarak sinterlenmiştir. Mevcut çalışmanın sonuçları magnezyum nanopartikülleri kullanılarak bakırın güçlendirilebileceğini göstermiştir. Cu yüksek sıcaklıklarda yumuşayan bir malzeme özelliği taşımaktadır. Bakıra MgO ekleyerek malzemenin farklı bir özellik gösterdiği ve sertliğinin arttığı gözlenmiştir. Görünür yoğunluk, hacimsel yoğunluk, mikroyapı, Vickers sertliği, mutlak gözeneklilik, EDS, su emme, termal iletkenlik, basınç dayanımı ve aşınma oranı gibi gerekli testler yapılmıştır. Ayrıca, kullanılan maddenin yapısını bulmak için SEM (Taramalı Elektron Mikroskobu) ve XRD (X-Işını Kırınımı) analizleri yapılmıştır.

**2023, 75 sayfa**

**Anahtar Kelimeler:** Fiziksel ve mekanik özellikler, Toz metalürjisi yöntemi

## PREFACE AND ACKNOWLEDGEMENTS

I would like to thank my thesis advisor Prof. Dr. Sebahaddin ALPTEKİN for his patience, guidance, and understanding. I would like to thank my dear husband for his support and assistance to me,

**Noor Jasim Zaboon AL-SAEDI**
**Çankırı-2023**

**CONTENTS**

## LIST OF SYMBOLS

| | |
|---|---|
| $\rho_a$ | Apparent density |
| $D_v$ | Average diameter |
| $W_s$ | Body weight is saturated with water |
| $^oC$ | Celsius Degrees |
| Cu | Cooper |
| D | Diameter of the disk |
| $\Theta$ | Diffraction angle |
| n | Diffraction peak (integer no) |
| d | Distance between atomic levels |
| $W_d$ | Dry weight |
| H | Hardness of material |
| P | Immediate load (kg) |
| $\Delta W$ | Lost weight |
| µm | Micrometer |
| ng | Nanogram |
| % | Percentage |
| $W_X$ | Vertical load sliding distance |
| $\rho_b$ | Volumetric density |
| $\rho_w$ | Water density |
| K | Wear coefficient (constant) |
| W | Wear rate |
| V | Wear volume |

## LIST OF ABBREVIATIONS

| | |
|---|---|
| AP | Apparent porosity |
| BD | Body density practical lactobacillus |
| CMCs | Metal matrix composites |
| EDS/EDX | Energy-dispersive X-ray spectroscopy |
| FCC | Face center cubic |
| Hv | Hardness Vickers |
| MgO | Magnesium oxide |
| MMCs | Ceramic matrix composites |
| PMCs | Polyme matrix composites |
| SD | Sliding distance |
| SEM | Scanning electron microscope |
| TD | Body density theoretically sintered |
| TP | True porosity |
| WA | Water absorption |
| XRD | X-ray diffraction |

**LIST OF FIGURES**

**LIST OF TABLES**

# 1. INTRODUCTION

The history and origin of interlaced materials stretch back to ancient civilizations known thousands of years ago. The Mesopotamian civilization was distinguished for being the first to know the use of interlocking materials. The Assyrians followed the principle of arming the building layers by using fibers from reeds to build the ziggurat interlocking materials that could be used in manufacturing. The history of copper cones in Türkiye stretches back to 7000 BC (Clyne and Withers 2003, Heba 2010). Excavations in the Çayönü Halls region of Türkiye, with the participation of the Universities of Istanbul and Chicago, found more than 40 free copper instruments found in layers dated 7250-6750 BC, and it is made up of Cones (Clyne and Withers 2003).

Pearls, clamps, small leaves, and wires, and through analyses that have grown on the sintering technique to a temperature of 500 m, can facilitate the process of roads and treat cracks caused by the road and become less prone to breakage. Overlapping materials have distinctive characteristics. These characteristics make them eligible to become essential materials in many advanced and current industries and complex technology in which substances have to meet industrial necessities in numerous areas, such as vehicles, planes, and thermal control areas of the thermal industry (Hedjazi 2009, Bruls 2002).

Moreover, the overlapping materials are a mixture of two or more substances, one of which is known as the matrix material base material or Phase Continuous. The second is known as Reinforcement Material or Distributed Phase. The phase that surrounds the base material could be metal, ceramic, or polymeric, but the reinforcement may be fiber, sheets, or bristles (Groover 2020).

The primary motivation of these materials is to increase the efficiency of mineral materials to retain all their features, such as high cutting resistance, and maintain good characteristics at high temperatures. Overlapping materials are the best specifications of the two articles individually, and the overlapping material is one mass.

Interest in overlapping materials began in previous years from various engineering materials to improve solidity and resistance, withstand high temperatures, and resistance to wear and tear (Miracle and Donaldson 2001). Overlays gain strength from the strengthening phase and the continuous phase or foundation connects the particles of strengthening material and transfers and distributes the load to it. Overlays depend on the components and proportions. The accumulated substances are classified into three varieties according to the base substance (Cardarelli 2008).

**Items:**

- Polymer Matrix Composites (PMCs)
- Ceramic Matrix Composites (MMCs)
- Metal Matrix Composites (CMCs)

In this study, we will take Metal Matrix Composites (MMCs), which defines advanced engineering as having the characteristics and advantages used in these super metallic posts as a base and supported by one of the strengthening phases such as particles, fiber bristles, and other reinforcement materials. The properties of these synthesized materials control, in general, both the base metal type and the type of reinforcement material added to its size, shape, location, and manufacturing method. When comparing metal superimposed materials with alloy or base metal without reinforcement, we will note the following features (Cardarelli 2008, Chawla and Chawla 2006):

- The high proportion of resistance
- The goodness of corrosion resistance.
- The improvement in high-temperature resistance.
- Tensile resistance is high.
- The rate of creep is low.
- The coefficient of thermal expansion is low.

In this study, we were asked to prepare copper and MgO compounds using metal powder technology and the effect of nano MgO content on the structural, physical and mechanical properties of compounds for testing. In this study, a significant role in manufacturing many applications is influenced by the following metal powder. It will help to understand the most critical features that affect that structure will include: SEM analysis, EDX analysis, grid constant, grain size, mechanical properties such as Vickers hardness, corrosion, and crawling and physical properties such as real and visible density, porous and visible water absorption. Check these variables before and after thermal sintering and study the impact of the added mixture ratios on all physical and mechanical properties.

## 2. LITERATURE REVIEW

In 2005, the researcher Wang and others in their study “The properties of the effects of copper supported by silicon carbide and alumina by powder technology and microscopy” showed that the overlay density decreases when alumina and silicon carbide molecules increase, and the density of the overlay Cu-$Al_2O_3$ is higher than the silicon carbide density Due to the high density of alumina (Wang *et al*. 2005).

In 2006, the researcher Griffin in his study “The production of copper pistons with powder technology and the study of the sintering process's impact on these pistons' general properties” showed that when the pressure load increases and the higher the temperature increases, the density increases (Griffin 2006).

In 2010, the researcher Nazarian-Samani in his study “The Changes in the powder phase were studied for 15% of NiB for alloys during the annealing process after the grinding process for different periods” caused that changes in the phases when the grinding process took place within 25 hours; the overlay changed to $Ni_3B$; when the grinding process continued for 40 hours, the phase changed to O-$Ni_4B$ and $Ni_2B$ (Nazarian-Samani *et al.* 2010).

In 2011, the researcher Younis in his study “The characteristics of the overlay of these Cu-Mg-Sic mechanical samples of copper base material and the addition of supporting material have been prepared SiC at a constant 25% using powder technology and adding magnesium at volume ratios (0-10)%” showed that with the increased ratio of magnesium element, there was an increase in the density of the samples. A decrease in porosity was also observed, in addition to improvements in the mechanical properties (Younis 2011).

In 2015, the researcher Balamurugan in his study “The wear properties of Al-SiC-$Al_2O_3$ were studied by adding different content of silicon carbide from 5% wt to 25% wt, and when the weight increased, the apparent porosity increased by 39% the 75% hardness

increased and both the 15% shock energy and relative density decreased 1.08%" (Balamurugan *et al*. 2015).

In 2016, the researchers Venkatesh and Harish in their study "The overlay characteristics were prepared and studied (Al-SiC) with different weight ratios of silicon carbide 2% wt - 8% wt. After pressing and mixing, the process of sintering the samples at 500 °C for two hours" showed that the higher the weight ratios of silicon carbide, the greater the hardness from 19.48% to 23.94% of the weight ratios (2% Sic–8% Sic) (Venkatesh and Harish 2016).

In 2019, the researcher Ali in his study "The study of the impact of SiC on some of the mechanical properties Of Ni. The base material in the sample was Al by adding a certain fixed percentage of Ni 20% and SiC to it in different ratios (4, 6, 8) % where all the powders were mixed and pressed 700Mp And then sintering. At 530 ℃" showed that hardness has increased by 52%, and the corrosion rate decreased by 55% when adding 8% SiC (Ali 2019)

In 2020, the researcher Gohar in her study "By powder technology Verified in synthetic and mechanical properties of alloys Cu-Al-Ni and the addition of silver. Cu was considered an essential material in the preparation of samples. A percentage of Al 10% and Ni 4% were added, and silver was added as a supporting material with different content and weight ratios ranging from (0.2%-4.6%). After mixing and pressing the samples, the sintering process took place at the temperature of 850 °C, after which the cooling process was carried out in three ways: Oven, water, and oil. After that, tests such as the electronic SEM scanner microscope, XRD and HR test, and Rockwell Hardness test" showed that the sample values were higher in water than in the oven and oil refrigeration process (Gohar *et al.* 2020).

# 3. MATERIALS AND METHODS

## 3.1 Copper

### 3.1.1 Copper properties

Copper is one of the first metals to be used by humans. It is a bright red metal, pure form after silver in electrical conductivity, and is widely used in the electrical and electronic industries; Figure 3.1 shows copper in powder form.

The chemical symbol of the element Cu, Atom number 29, Atomic weight (63.54 g/mol), and crystal structure FCC have high corrosion resistance and the ability to form. It has high corrosion resistance and formation capacity and is one of the metals widely used in many engineering industries. Due to its thermal properties, it is widely used in electrical, mechanical, construction, and household chores on its good conductivity at high and low temperatures. It is reasonably priced and can be recycled and not ignited.

The earth has a median copper content material of about 0.006% and is a common element as it is the 23rd most common component of the earth, and in almost all types of rocks, there are traces of copper. Copper is protected within the first subset of the periodic table at the side of silver and gold (Lipowsky and Arpaci 2008).


**Figure 3.1** Copper in powder form

However, it undergoes the problem of softening at the highest temperatures, which in this study was reinforced by nano MgO with excellent qualities to improve some copper properties. Natural copper's most critical and beneficial physical qualities are its immoderate thermal and electric-powered conductivity after silver. Table 3.1 shows the physical properties of pure copper at 20 °C (Lipowsky and Arpaci 2008).

**Table 3.1** The physical properties of pure copper at 20 °C

| **Physical property** | **Measured value** | **Units** |
|---|---|---|
| Lattice constant | 0.3608 | nm |
| Density (highly pure copper at 99.999% Cu) | 8.959 | $g/cm^3$ |
| Volume defect on solidifying | 4.9 | % |
| Melting point | 1083 | °C |
| Fusion heat | 214 | J/g |
| Evaporation heat | 4770 | J/g |
| Boiling point | 2595 | °C |
| Heat conductivity at RT | >385 | W/m·K |
| Electrical conductivity at RT | 59.62 | MS/m |
| Young's modulus for wrought material | 100000–130000 | $N/mm^2$ |

### 3.1.2 Copper uses

The most critical applications of copper (Lipowsky and Arpaci 2008);

- It is widely used for domestic purposes, valves, water tanks, and pipes.
- It is included in manufacturing counterfeit ornaments, coins, and some decorations as it is one of the primary metals.
- It is used frequently in the manufacture of fuel-equipped engines and oil pipes.
- In modern technology, it has become an essential material for its use in the manufacture of advanced railway vehicles and silicon chips.
- It represents the main element in the manufacture of bullet casings.

- It is used to manufacture heat exchange tubes, condensates, and electric brushes.
- It included the cable industry and some distribution lines to transport electricity.
- It includes the production of many valuable alloys, such as Cu-Ni alloy, which is used in the manufacture of submarines and ships because it has high resistance to corrosion
- It enters the manufacture of bronze.

## 3.2 Nano-Magnesium Oxide

### 3.2.1 Magnesium oxide properties

The MgO partial version is also called magnesia. It is a white, odorless compound found in nature in the form of Periclase. It must be kept in sealed containers because it can interact with other elements to produce new elements that may be dangerous or produce toxic gases.

Even though "magnesium oxide" typically means MgO, $MgO_2$ magnesium peroxide is also called a mixture. Based on evolutional crystalline shape estimates, $MgO_2$ is thermodynamically solid at pressures more than 116 GPa (gigapascals), and it became a semiconductor oxidizer is thermodynamically solid at $Mg_3O_2$ 500 GPa for reasons of its balance (Zhu *et al.* 2013).

MgO is employed as a version machine for investigating the vibratory of crystals (Mei *et al.* 2015).

Calcination At distinctive temperatures produces MgO with specific reagents. High temperatures between 1500 °C and 2000 °C reduce the to-be-had superficial area and produce useless burnt magnesia, regularly referred to as "lifeless combustion," a non-reactive Shape used as a refractory. Calcination temperatures between a thousand and 1500 °C. Produce hard magnesia, a reactive shape called caustic calcined magnesia, which has restrained reactivity temperature calcination 700 °C to 1000 °C. While a few carbonate oxidation happens at temperatures below 700 °C, the consequent materials seem to excrete carbon dioxide from the air (Figure 3.2) (Table 3.2) (Ropp 2012).


**Figure 3.2** MgO in powder form

**Table 3.2** MgO properties (Haynes *et al.* 2016, Taurian *et al.* 1985)

| **Molar mass** | **40.304 g/mol** |
|---|---|
| Appearance | White powder |
| Odor | Odorless |
| Density | 3.6 g/cm$^3$ |
| Melting point | 2,852 °C (5,166 °F; 3,125 K) |
| Boiling point | 3,600 °C (6,510°F; 3,870 K) |
| Solubility | Soluble in acid, ammonia insoluble in alcohol |
| Band gap | 7.8 eV |
| Magnetic susceptibility ($\chi$) | $-10.2\cdot10^{-6}$ cm$^3$/mol |
| Thermal conductivity | 45–60 W·m$^{-1}$·K$^{-1}$ |
| Refractive index ($n_D$) | 1.7355 |
| Dipole moment | 6.2 ± 0.6 D |

### 3.2.2 Magnesium oxide uses

Nano-materials are materials ranging in size from (1-100) nm, which show unique and new qualities different from the materials from which they were produced (Vigneshwaran *et al.* 2018).

This consideration makes them materials widely involved in aspects of life and technology industries such as medical biology electronics catalysts and solar energy interactions (Saha *et al.* 2017).

Magnesium oxide is a significant substance with a wide spread in the field of nanotechnology because of its use as a catalyst for reactions and treatment of toxic waste (Kandiban *et al*. 2015).

The researchers have conducted many studies in the past and recently in treatment, paint and superconducting products, and antibacterial activities and which inorganic substances have been integrated with polymers acting as mechanical enhancers, thermal catalysts, and antioxidants (Abdel-Wahab *et al.* 2017).

## 3.3 Method

Powder metallurgy technology has been used mainly for tungsten and molybdenum metals and their alloys, tungsten carbide and molybdenum carbide with super hardness and high melting points for metals and alloys that cannot be created by mechanical forming or machining.

Aluminum, copper, and alloys above melting temperature of 2000 °C problems of industrial production of parts made of melt-resistant metals are manufactured today based on the number of fast parts (Chawla and Chawla 2006).

Purity of the chemical composition of alloys and materials used in powder metallurgy and accuracy is of great importance since a combination of certain materials is highly purified, it is possible to obtain, and the process of product preparation does not involve combustion. For compounds or alloys, using powder metallurgy methods in manufacturing various product materials significantly saves more and thus dramatically reduces the costs of finished products. This method is one of the common production processes in Türkiye, economically viable, and one of the most important fields of material science has been made. Powder metallurgy technology is summarized in the following steps (Lee *et al*. 1998).

1-Mineral powders by mechanical methods (grinding, and freezing) or chemical methods preparation (dust from specific chemical reactions) and the water atomization System. There are more complex methods, including. Specific to products determined by the beneficiary, mixing or blending powders of different metals to obtain properties is possible.

2-Pressing of powders using pistons in molds that give the desired shape or form, briquettes characterized by high strength and resistance, and particles during the pressing of dust gaps between them are reduced, and some cohesion occurs between them.

3- Sintering cold pressed products by heating them to relatively high temperatures, but these melting of metals are always located at the melting temperature of the powder metal or in the composition of the powder temperature. Sintering leads to the merging of particles, resulting in high product density and resistance. A suitable temperature and time selection should be made.

Powders used in this article were desiccated at a temperature of 200 °C for one hour to do away with moisture and different unstable substances. After completing the milling and mixing process for a couple of hours using a laboratory mill containing metallic balls, as shown in Figure 3.3


**Figure 3.3** A laboratory mill containing metallic balls

A homogeneous powder has acquired the specimens were fashioned with a uniaxial compaction technique in stainless steel. The milled aggregate was placed internal compaction template, which was placed very carefully and as it should be to save any transportation of the template parts. Then, a load of 5 tons becomes pressured for one minute to avoid the possibility of elastic pressure. For this purpose, hydraulic compaction with a load of 20 tons is used to reap cylindrical specimens, as shown in Figure 3.4 (Chawla and Chawla 2006).

**Figure 3.4** A Specimen

Sintering into accomplishe oven at a temperature 900 °C for couple hours (Figure 3.5).

**Figure 3.5** Accomplishe oven

## 3.4 Raw Materials (Powders)

The metal powder has been used to prepare composite materials copper is the base material, copper Cu, with an atom size of (63 μm) of German origin, manufactured by Riedel-Dehaenag Seelze-Hannover Company, with a purity of 99.5%. Also used of the reinforcement material was manganese MgO with an atom size of (20 μm) of USA origin from US Research Nanomaterial, Inc. company with a purity of 99%.

## 3.5 Preparing and Testing Specimens

As seen in Figure 3.6, the steps in sequence and the stages that were done in this study and the tests and tests that were conducted.

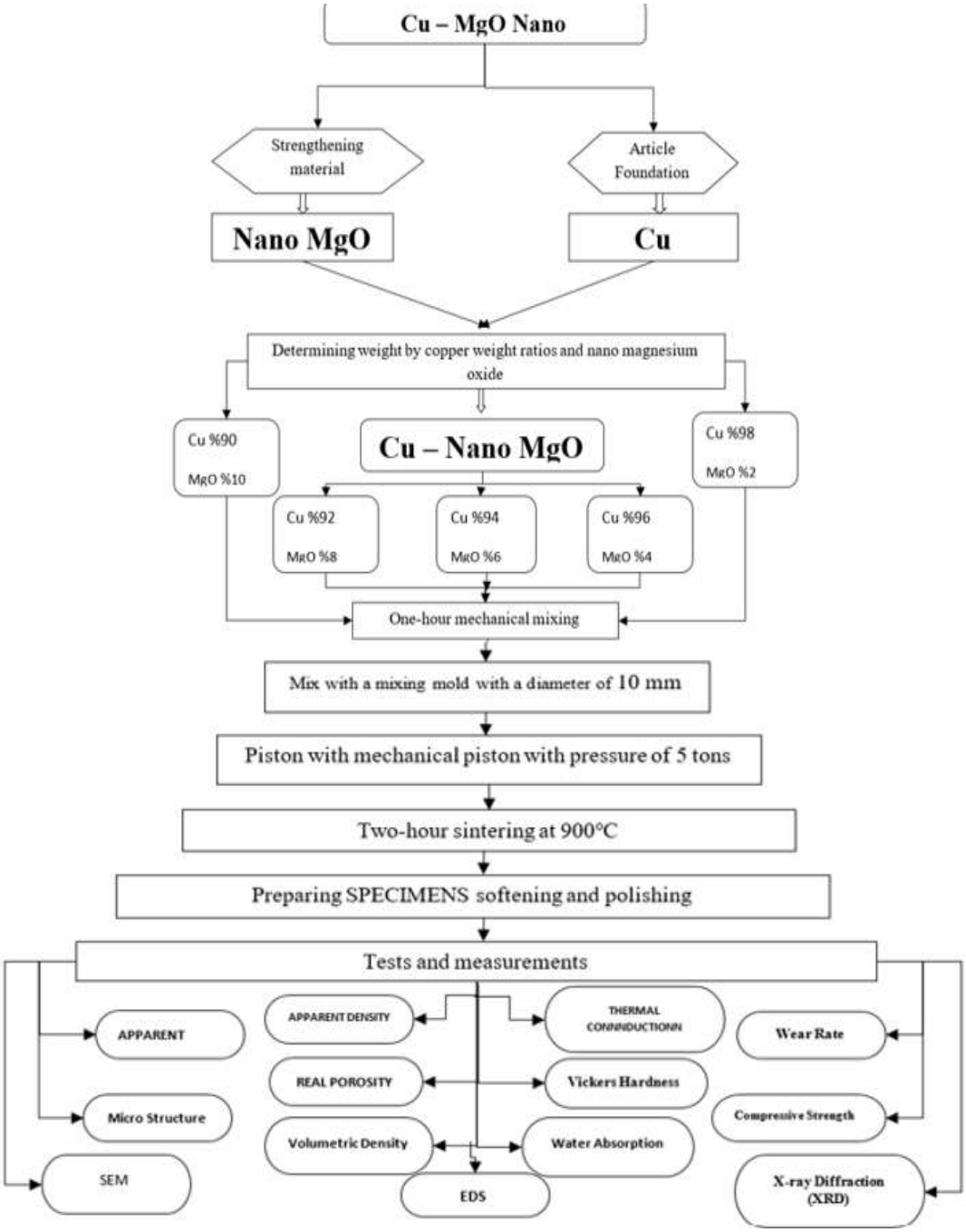


**Figure 3.6** Working scheme

In this study, we mixed powders in the grinding process to obtain superimposed materials with specific weight ratios of the base material and reinforce them with the weight ratios of the reinforcement material. This process aims to systematically and homogeneously distribute different volumes of powders, and during this process, there is a collision between two hard spheres with two small particles between them.

The impact force of these spheres resulted in the breakdown and deformation of the molecule and the adhesion of its particles consisting of large, homogeneous particles in the form of layers, (Figure 3.7) (Upadhyaya 1997).

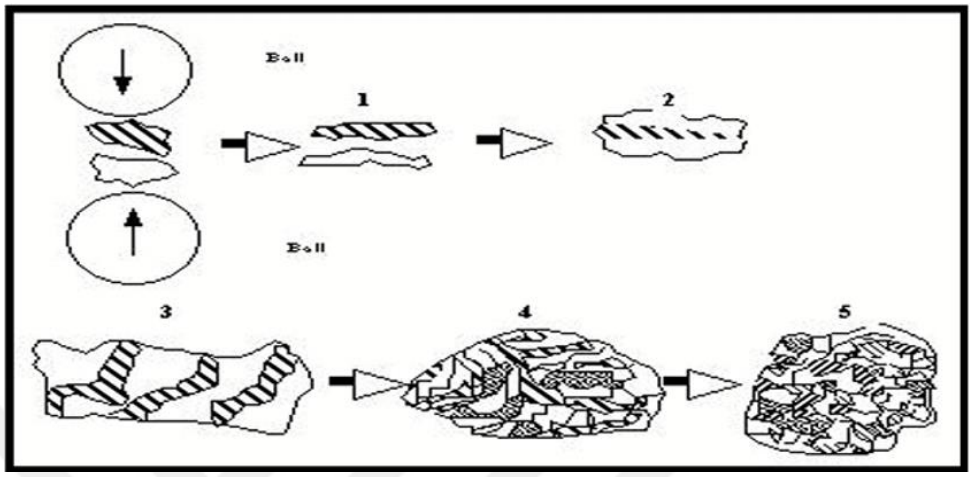


**Figure 3.7** Powder between the two grinding balls during the grinding process

After completing the milling and mixing process for a couple of hours using a laboratory mill containing metallic balls, a homogeneous powder was received. The specimens had been shaped by the use of a uniaxial compaction approach (Figure 3.8).

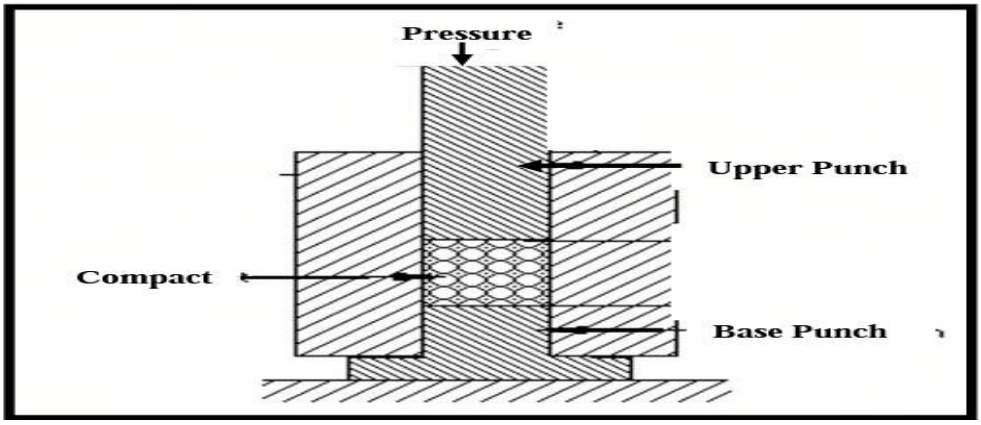


**Figure 3.8** Uniaxial compaction (Al-Sharifi 2007)

Stainless steel can be a template of 60 HRC, and the milled combination becomes positioned inner compaction, which was positioned very cautiously and accurately to prevent Any motion of the Template components. Then, a load of five tons was forced for one minute to avoid the potential of elastic stress (Chawla and Chawla 2006).

For this motive, A Turkish-starting place hydraulic compaction of HALIM USTA with a load of 20 tons changed into used to attain cylindrical specimens with a diameter of 10 mm and peak of 6 mm (Figure 3.9).

**Figure 3.9** Hydraulic compaction of HALIM USTA

After compaction, We put the specimens in the oven at 900 °C for two hours. As seen in Figure 3.10, changes in structure during the sintering process.

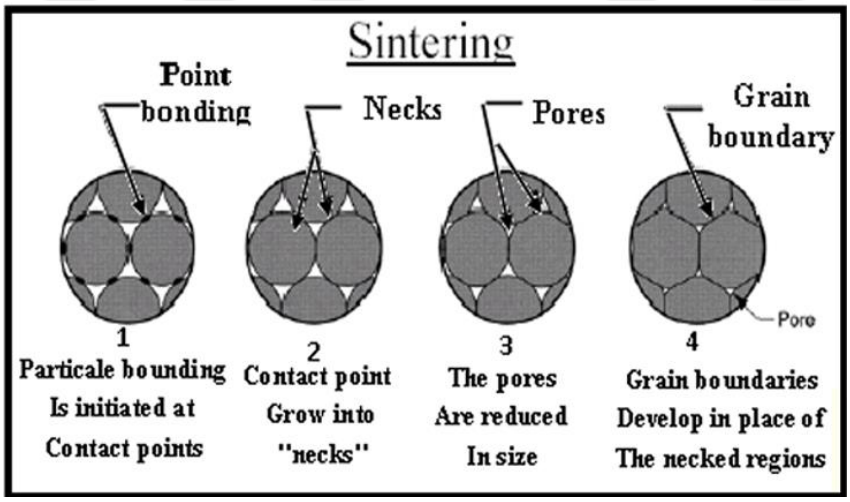


**Figure 3.10** Changes in the structure during the sintering process (Groover 2020)

Changes in the structure during the sintering process Which is the adhesion of the powder pellets at the contact points show a result that at the contact points, the hugs form, and then the diminution in the size of the pores begins. There is a decrease in the number of pores, and then a crystal boundary arises in these regions.

This sintering process has a direct and significant impact on the properties of the resulting substances hardening, conductivity, porosity, and many other properties and the sintering stages (Figure 3.11).

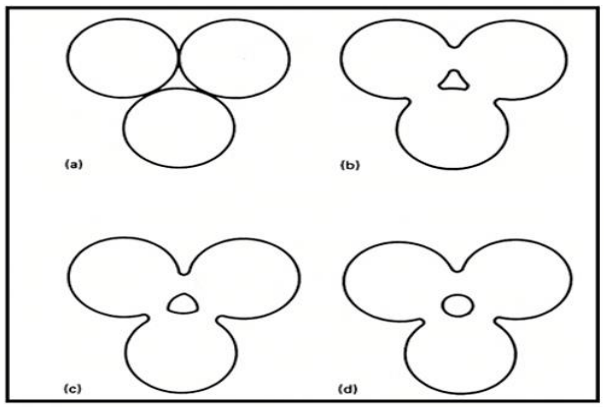


**(a)Original Point Contacts (b)Neck Growth (c) and (d) Pore Rounding**

**Figure 3.11** Phases of the sintering process (Wu *et al.* 2004)

When the pores in the pressed materials begin to shrink in size due to adaptation, there will be no spaces at these stages. The pores cannot be removed either during the sintering process, and some pores remain even after long sintering.

# 4. TESTS AND MEASUREMENTS

## 4.1 Vickers Hardness Test

Micro-hardness is one of the most important mechanical properties, defined as the surface indentation obtained by the material (Jin and Hu 2011).

The hardness was the use of the Vickers method with the aid of putting a rectangular-footed diamond pyramid onto the organized patterns. Specimens were tested using a device (Digital Hardness Brinell, Rockwall, Vickers Tester HBRVS-187.5 Chinese Laryee CO. (Figure 4.1) (Figure 4.2).


**Figure 4.1** Digital Hardness Brinell, Rockwall, Vickers Tester HBRVS-187.5 Chinese Laryee CO (I)

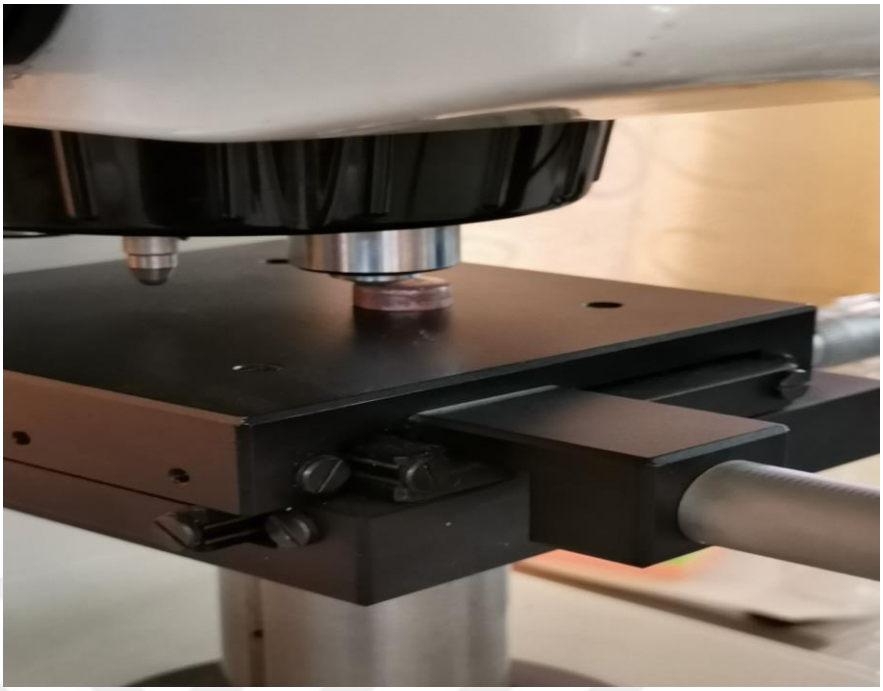

**Figure 4.2** Digital Hardness Brinell, Rockwall, Vickers Tester HBRVS-187.5 Chinese Laryee CO (II)

Via shedding the device with a mass of 500 gm and a time (10 sec), and when calculating the diameters of the ensuing trace on the floor, the hardness values of the specimens can be known by applying the in Equation (4.1) according to the following;

$$Hv=1.8544\ P/D^2_V\ Kg/mm^2 \qquad (4.1)$$

If:

- P = Immediate load (Kg)
- Dv = the average diameter of the pyramidal effect attributable to the weight being shed onto the surface (Figure 4.3) (Table 4.1).

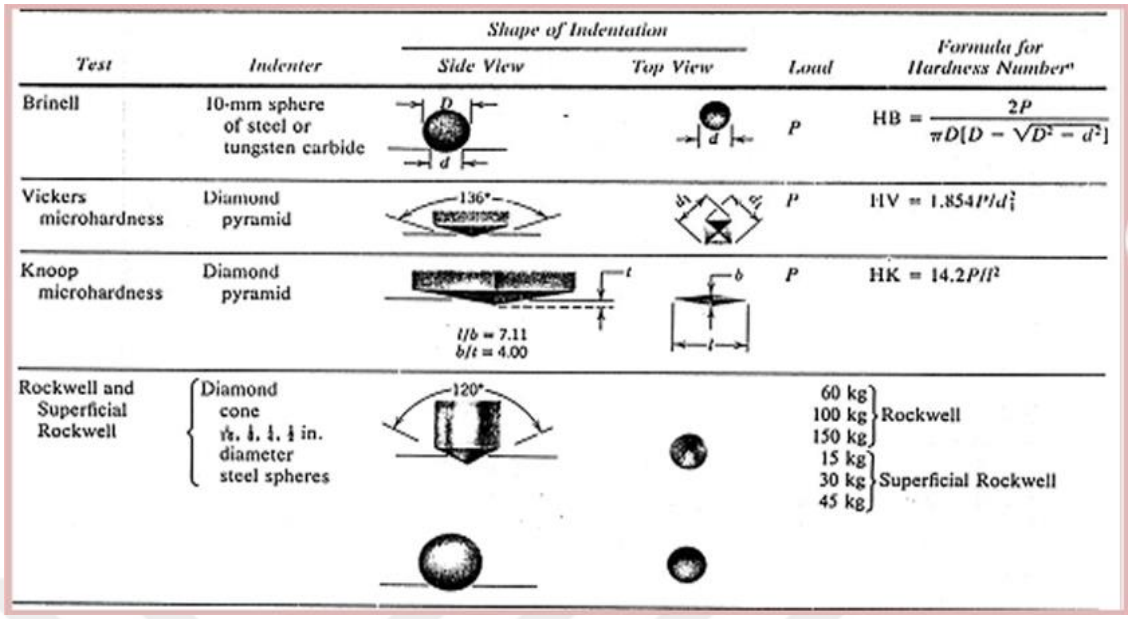


**Figure 4.3** Different ways to test hardness (Giri *et al.* 2021)

**Table 4.1** Vickers Hardness test results before and after sintering process

| MgO % | Solidity before (2) hours | Solidity after (2) hours |
|---|---|---|
| 2 | 39 | 66 |
| 4 | 44 | 78 |
| 6 | 51 | 85 |
| 8 | 67 | 110 |
| 10 | 88 | 118 |
| Grinding time | 2 | |

## 4.2 Wear Rate Test

The wear Rate Test is one of the most important mechanical properties of the material. It is defined as the loss of material from the metal surface due to the friction of moving parts (Figure 4.6) (Figure 4.7) (Figure 4.8) (Figure 4.9) (Figure 4.10) (Figure 4.11) (Figure 4.12) (Figure 4.13) (Figure 4.14) (Figure 4.15). This test was performed using a homemade device

Preliminary experiments determined the amount of pregnancy applied 10 N, using a constant sliding speed of 480 rpm, and the pregnancy period for each test changed to 10 minutes. Table 4.2 explains corrosion conditions (Lee *et al*. 1998).

$$W = \frac{\Delta W}{SD} \text{ (g/cm)} \quad (4.2)$$

Where (W) is weight (g/cm), (ΔW) is lost weight (gm) and represents the distinction in weight of the pattern before and after operation, (SD) represents sliding distance (cm), which is same to Equation (4.3):

$$SD = \pi D n t \quad (4.3)$$

Where (D) represents the diameter of the disk (cm), (n) represents the rotational speed of the disk (rpm), and (t) is test time (min).

**Table 4.2** Wear rate test conditions

| **Rotational velocity of the disc** | **480 rpm** |
|---|---|
| Test time | 10 min |
| Vertical load implemented | 10 N |
| Diameter of take a look at disc | 60 mm |
| Disk hardness | 62 HRC |

**Test Steps**

- Preparing compacted specimens with a diameter of 10 mm and a height of 5 mm.
- Grinding compacted specimens using sandpaper (400, 600, 800, 1200) MPa.
- Weighing compacted specimens earlier than the test using a touchy digital balance.
- Cleaning the disc of the device before beginning the task.
- Solving loads and applying a load of (15, 20, 25) Newton vertically to compacted specimens at a rotational pace of the disk (480 rpm).
- Starting device after setup the take a look at time to zero.
- Stopping the device 20 minutes after its start.
- Casting off and weighing compacted specimens in the stability after the check.
- Determining the amount of weight reduction.

- Making use of connection 3 to extract the wear and tear charge for every compacted specimen.
- The above process had been recurrent for all compacted specimens, and the wear value was calculated for each compacted pattern by using calculating the average wear value for the pinnacle and backside surface of every compacted specimen (Table 4.3).

**Table 4.3** Wear rate test results before and after sintering process

| MgO % | Wear out before (2 hours) | Wear out after (2 hours) |
|---|---|---|
| 2 | 3.43E-04 | 2.12E-04 |
| 4 | 2.03E-04 | 5.96E-05 |
| 6 | 1.52E-04 | 3.15E-05 |
| 8 | 1.04E-04 | 1.33E-05 |
| 10 | 5.20E-05 | 1.06E-05 |
| Grinding time | 2 | |

## 4.3 Compressive Strength Test

Compressive strength is one of the important mechanical properties, representing the ability of compacted materials to withstand the loads applied to them. Compacted specimens were tested using the device of (Laryee Technology CO, LTD–WDW-100) Chinese Origin (Figure 4.4).

**Figure 4.4** Laryee Technology CO, Ltd–WDW-100

After compacting and grinding specimens using sandpaper with more than a few (four hundred to two thousand) MPa micrometers, they were constant between the jaws of the tool, and then load changed into applicable them until failure through strain-stress curve drawn using the device. The values of compressive strain were extracted (б 0.2) from drawing (Figure 4.5) (Table 4.4) (Table 4.5) (Table 4.6) (Table 4.7) (Table 4.8) (Table 4.9).

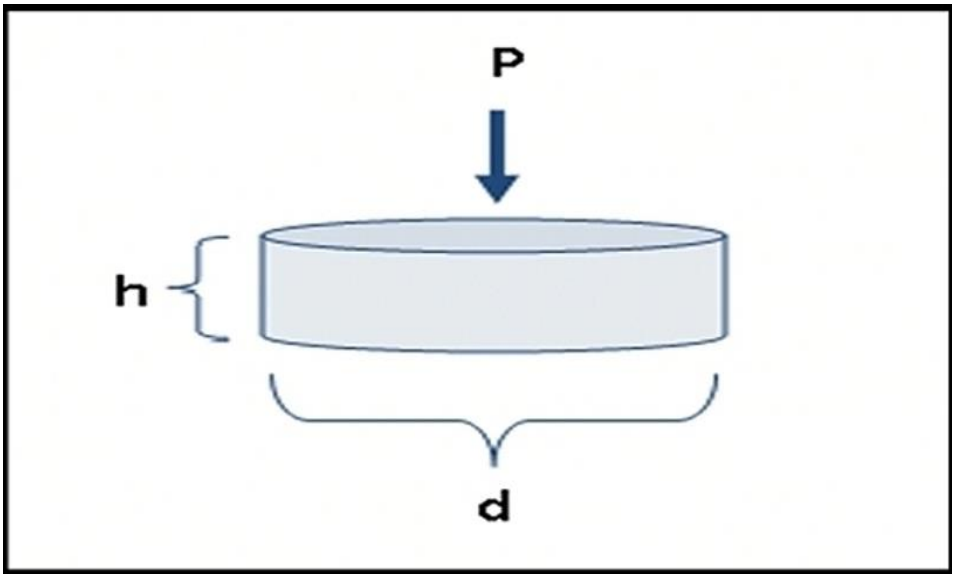


**Figure 4.5** Specimen dimension

**Table 4.4** Compressive strength test results before and after sintering process

| MgO % | Resistance compression before (2 hours) | Resistance compression after (2 hours) |
|---|---|---|
| 2 | 22 | 39 |
| 4 | 26 | 44 |
| 6 | 33 | 51 |
| 8 | 40 | 57 |
| 10 | 45 | 63 |
| Grinding time | 2 | |

**Table 4.5** Compressive strength values (Stress Strain Curve) for Specimen 1

| S1NO | SampleID |
|---|---|
| 1.04.2022 | TestDate |
| S1NO | Operator |
| Circle | Type |
| 10 | Size(mm) |
| 20.76 | Fbc(kN) |
| 173 | Rbc(MPa) |
| 17.90 | Fsc(kN) |
| 149 | Rsc(MPa) |
| 0.60 | Ftc(kN) |
| 5 | Rtc(MPa) |
| 1.13 | Ec(GPa) |
| | |
| | |
| | |
| ----------Curve---------- | |
| | |

| Time | Load | Elong | Displacement | Stress | Strain | Width |
|---|---|---|---|---|---|---|
| 0 | 0.000 | 0.000 | 0.001- | 0.000 | 0.000 | 0.000 |
| 4.013 | 0.245 | 0.125 | 0.130- | 2.045 | 0.250 | 1.000- |
| 7.748 | 0.600 | 0.250 | 0.254- | 5.009 | 0.500 | 1.000- |
| 11.5 | 0.955 | 0.375 | 0.380- | 7.972 | 0.750 | 1.000- |
| 15.235 | 1.220 | 0.500 | 0.504- | 10.184 | 1.000 | 1.000- |
| 18.949 | 1.375 | 0.625 | 0.629- | 11.478 | 1.250 | 1.000- |
| 22.682 | 1.580 | 0.750 | 0.754- | 13.190 | 1.500 | 1.000- |
| 26.396 | 1.835 | 0.875 | 0.879- | 15.318 | 1.750 | 1.000- |
| 30.13 | 2.170 | 1.000 | 1.004- | 18.115 | 2.000 | 1.000- |
| 33.824 | 2.490 | 1.125 | 1.129- | 20.786 | 2.250 | 1.000- |
| 37.558 | 2.810 | 1.250 | 1.254- | 23.458 | 2.500 | 1.000- |
| 41.251 | 3.115 | 1.375 | 1.379- | 26.004 | 2.750 | 1.000- |
| 45.005 | 3.420 | 1.500 | 1.504- | 28.550 | 3.000 | 1.000- |
| 48.719 | 3.720 | 1.625 | 1.629- | 31.054 | 3.250 | 1.000- |
| 52.453 | 4.015 | 1.750 | 1.754- | 33.517 | 3.500 | 1.000- |
| 56.166 | 4.300 | 1.875 | 1.879- | 35.896 | 3.750 | 1.000- |
| 59.92 | 4.580 | 2.000 | 2.004- | 38.234 | 4.000 | 1.000- |
| 63.655 | 4.860 | 2.125 | 2.130- | 40.571 | 4.250 | 1.000- |
| 67.388 | 5.130 | 2.250 | 2.254- | 42.825 | 4.500 | 1.000- |
| 71.082 | 5.395 | 2.375 | 2.379- | 45.037 | 4.750 | 1.000- |

**Table 4.5** Compressive strength values (Stress Strain Curve) for Specimen 1 (Continued)

| Time | Load | Elong | Displacement | Stress | Strain | Width |
|---|---|---|---|---|---|---|
| 74.835 | 5.670 | 2.500 | 2.504- | 47.333 | 5.000 | 1.000- |
| 78.57 | 5.950 | 2.625 | 2.630- | 49.670 | 5.250 | 1.000- |
| 82.284 | 6.220 | 2.750 | 2.754- | 51.924 | 5.500 | 1.000- |
| 86.038 | 6.495 | 2.875 | 2.880- | 54.220 | 5.750 | 1.000- |
| 89.771 | 6.775 | 3.000 | 3.004- | 56.557 | 6.000 | 1.000- |
| 93.485 | 7.050 | 3.125 | 3.129- | 58.853 | 6.250 | 1.000- |
| 97.258 | 7.340 | 3.250 | 3.254- | 61.274 | 6.500 | 1.000- |
| 101.012 | 7.625 | 3.375 | -3.379 | 63.653 | 6.750 | -1.000 |
| 101.033 | 7.625 | 3.375 | 3.380- | 63.653 | 6.750 | 1.000- |
| 104.786 | 7.920 | 3.500 | 3.504- | 66.116 | 7.000 | 1.000- |
| 108.56 | 8.230 | 3.625 | 3.630- | 68.704 | 7.250 | 1.000- |
| 112.293 | 8.550 | 3.750 | 3.754- | 71.375 | 7.500 | 1.000- |
| 116.047 | 8.875 | 3.875 | 3.879- | 74.088 | 7.750 | 1.000- |
| 119.801 | 9.205 | 4.000 | 4.004- | 76.843 | 8.000 | 1.000- |
| 123.535 | 9.540 | 4.125 | 4.129- | 79.639 | 8.250 | 1.000- |
| 127.289 | 9.895 | 4.250 | 4.254- | 82.603 | 8.500 | 1.000- |
| 131.042 | 10.250 | 4.375 | 4.380- | 85.566 | 8.750 | 1.000- |
| 134.777 | 10.620 | 4.500 | 4.504- | 88.655 | 9.000 | 1.000- |
| 138.53 | 10.990 | 4.625 | 4.629- | 91.744 | 9.250 | 1.000- |
| 142.264 | 11.370 | 4.750 | 4.754- | 94.916 | 9.500 | 1.000- |
| 146.017 | 11.740 | 4.875 | 4.879- | 98.005 | 9.750 | 1.000- |
| 149.771 | 12.110 | 5.000 | 5.004- | 101.094 | 10.000 | 1.000- |
| 153.505 | 12.510 | 5.125 | 5.129- | 104.433 | 10.250 | 1.000- |
| 157.239 | 12.910 | 5.250 | 5.254- | 107.772 | 10.500 | 1.000- |
| 160.953 | 13.320 | 5.375 | 5.379- | 111.195 | 10.750 | 1.000- |
| 164.687 | 13.760 | 5.500 | 5.504- | 114.868 | 11.000 | 1.000- |
| 168.4 | 14.190 | 5.625 | 5.629- | 118.457 | 11.250 | 1.000- |
| 172.114 | 14.650 | 5.750 | 5.754- | 122.297 | 11.500 | 1.000- |
| 175.848 | 15.120 | 5.875 | 5.880- | 126.221 | 11.750 | 1.000- |
| 179.562 | 15.600 | 6.000 | 6.004- | 130.228 | 12.000 | 1.000- |
| 183.277 | 16.070 | 6.125 | 6.129- | 134.151 | 12.250 | 1.000- |
| 187.009 | 16.550 | 6.250 | 6.254- | 138.158 | 12.500 | 1.000- |
| 190.744 | 17.030 | 6.375 | 6.380- | 142.165 | 12.750 | 1.000- |
| 194.477 | 17.490 | 6.500 | 6.504- | 146.006 | 13.000 | 1.000- |
| 198.191 | 17.970 | 6.625 | 6.630- | 150.013 | 13.250 | 1.000- |
| 201.924 | 18.420 | 6.750 | 6.754- | 153.769 | 13.500 | 1.000- |
| 205.638 | 18.900 | 6.875 | 6.879- | 157.776 | 13.750 | 1.000- |
| 209.373 | 19.370 | 7.000 | 7.004- | 161.700 | 14.000 | 1.000- |
| 213.066 | 19.880 | 7.125 | 7.129- | 165.957 | 14.250 | 1.000- |
| 216.8 | 20.420 | 7.250 | 7.254- | 170.465 | 14.500 | 1.000- |
| 218.936 | 20.760 | 7.322 | 7.326- | 173.303 | 14.644 | 1.000- |

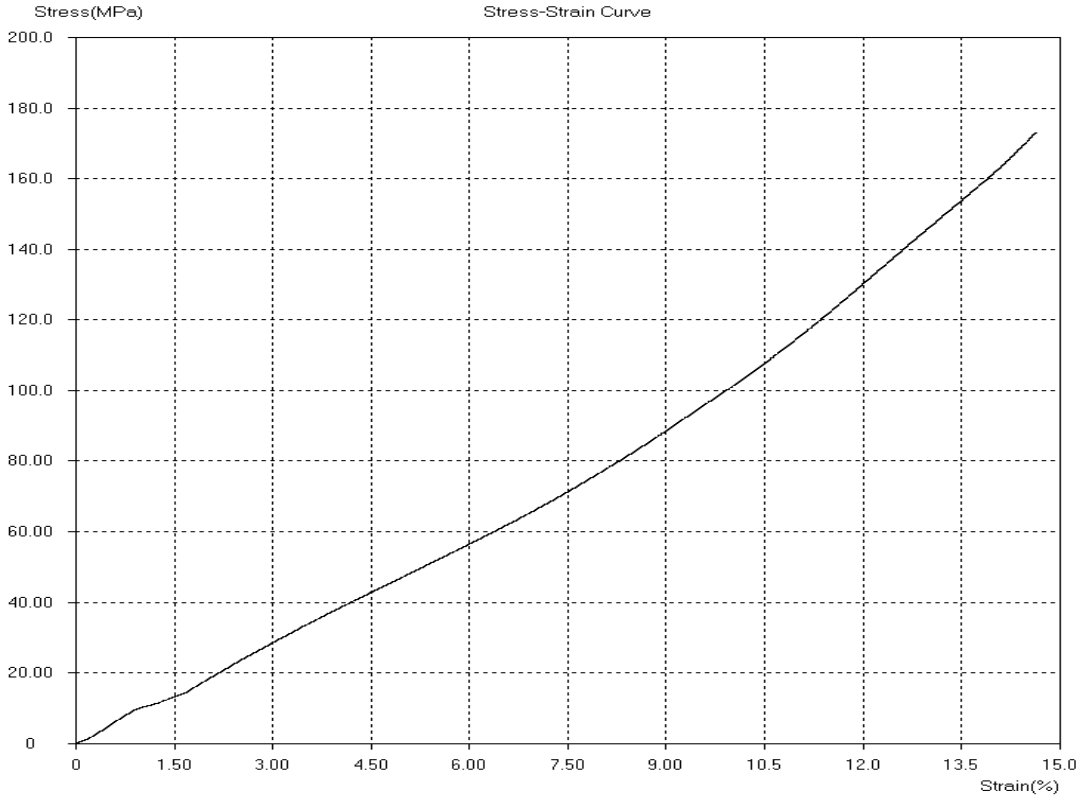


**Figure 4.6** Compressive strength (Stress Strain Curve) for Specimen 1

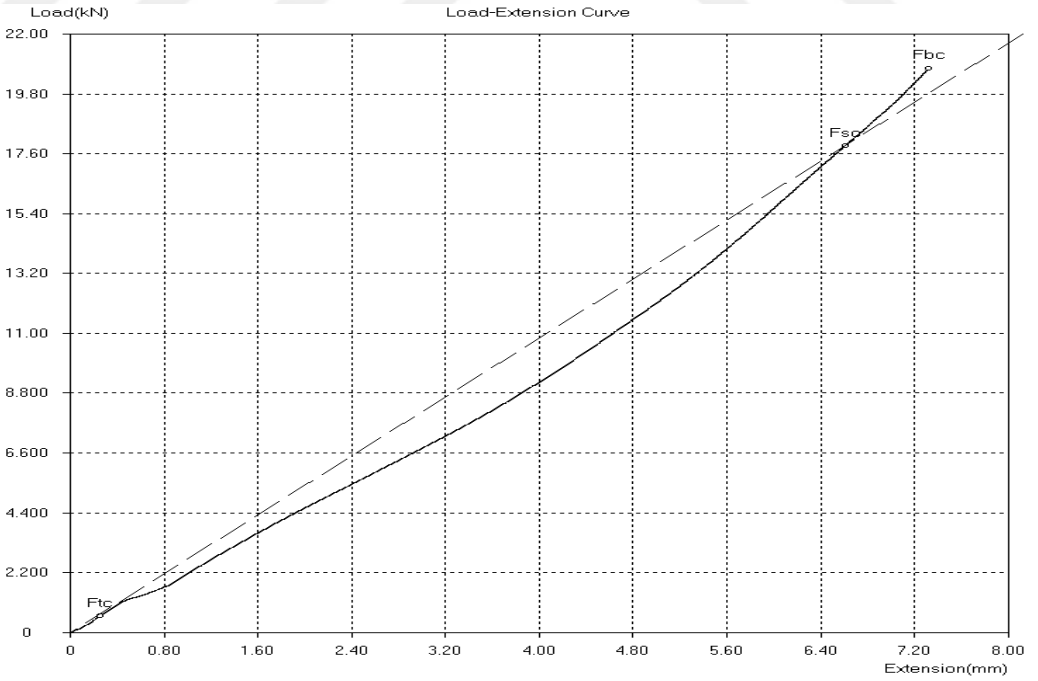


**Figure 4.7** Compressive strength (Load Extension Curve) for Specimen 1

**Table 4.6** Compressive strength values (Stress Strain Curve) for Specimen 2

| **S2NO** | **SampleID** |
|---|---|
| 1.04.2022 | TestDate |
| S2NO | Operator |
| Circle | Type |
| 10 | Size(mm) |
| 8.68 | Fbc(kN) |
| 72 | Rbc(MPa) |
| 4.54 | Fsc(kN) |
| 38 | Rsc(MPa) |
| 4.51 | Fpc(kN) |
| 38 | Rpc(MPa) |
| 1.10 | Ftc(kN) |
| 9 | Rtc(MPa) |
| 0.67 | Ec(GPa) |

----------Curve----------

| **Time** | **Load** | **Elong** | **Displacement** | **Stress** | **Strain** | **Width** |
|---|---|---|---|---|---|---|
| 0 | 0.000 | 0.000 | 0.002- | 0.000 | 0.000 | 0.000 |
| 4.014 | 0.605 | 0.125 | 0.130- | 5.051 | 0.250 | 1.000- |
| 7.768 | 1.095 | 0.250 | 0.256- | 9.141 | 0.500 | 1.000- |
| 11.501 | 1.610 | 0.375 | 0.380- | 13.440 | 0.750 | 1.000- |
| 15.255 | 2.055 | 0.500 | 0.506- | 17.155 | 1.000 | 1.000- |
| 18.969 | 2.410 | 0.625 | 0.630- | 20.119 | 1.250 | 1.000- |
| 22.702 | 2.730 | 0.750 | 0.756- | 22.790 | 1.500 | 1.000- |
| 26.436 | 3.025 | 0.875 | 0.881- | 25.253 | 1.750 | 1.000- |
| 30.15 | 3.290 | 1.000 | 1.006- | 27.465 | 2.000 | 1.000- |
| 33.864 | 3.535 | 1.125 | 1.130- | 29.510 | 2.250 | 1.000- |
| 37.578 | 3.760 | 1.250 | 1.256- | 31.388 | 2.500 | 1.000- |
| 41.292 | 3.970 | 1.375 | 1.380- | 33.141 | 2.750 | 1.000- |
| 41.311 | 3.970 | 1.375 | 1.381- | 33.141 | 2.750 | 1.000- |
| 45.025 | 4.160 | 1.500 | 1.506- | 34.727 | 3.000 | 1.000- |
| 48.759 | 4.335 | 1.625 | 1.630- | 36.188 | 3.250 | 1.000- |
| 52.493 | 4.465 | 1.750 | 1.756- | 37.274 | 3.500 | 1.000- |
| 56.227 | 4.545 | 1.875 | 1.880- | 37.941 | 3.750 | 1.000- |
| 59.961 | 4.615 | 2.000 | 2.006- | 38.526 | 4.000 | 1.000- |
| 63.694 | 4.660 | 2.125 | 2.130- | 38.901 | 4.250 | 1.000- |
| 67.428 | 4.625 | 2.250 | 2.256- | 38.609 | 4.500 | 1.000- |
| 71.142 | 4.545 | 2.375 | 2.380- | 37.941 | 4.750 | 1.000- |
| 74.895 | 4.620 | 2.500 | 2.506- | 38.567 | 5.000 | 1.000- |
| 78.609 | 4.725 | 2.625 | 2.630- | 39.444 | 5.250 | 1.000- |
| 82.344 | 4.840 | 2.750 | 2.756- | 40.404 | 5.500 | 1.000- |
| 86.077 | 4.975 | 2.875 | 2.880- | 41.531 | 5.750 | 1.000- |
| 89.831 | 5.110 | 3.000 | 3.006- | 42.658 | 6.000 | 1.000- |
| 93.585 | 5.255 | 3.125 | 3.131- | 43.868 | 6.250 | 1.000- |
| 97.339 | 5.375 | 3.250 | 3.256- | 44.870 | 6.500 | 1.000- |
| 101.072 | 5.475 | 3.375 | 3.380- | 45.705 | 6.750 | 1.000- |
| 104.846 | 5.540 | 3.500 | 3.506- | 46.248 | 7.000 | 1.000- |
| 108.6 | 5.560 | 3.625 | 3.630- | 46.415 | 7.250 | 1.000- |
| 112.373 | 5.600 | 3.750 | 3.756- | 46.748 | 7.500 | 1.000- |
| 116.107 | 5.615 | 3.875 | 3.880- | 46.874 | 7.750 | 1.000- |

**Table 4.6** Compressive strength values (Stress Strain Curve) for Specimen 2 (Continued)

| Time | Load | Elong | Displacement | Stress | Strain | Width |
|---|---|---|---|---|---|---|
| 119.881 | 5.610 | 4.000 | 4.006- | 46.832 | 8.000 | 1.000- |
| 123.615 | 5.635 | 4.125 | 4.130- | 47.041 | 8.250 | 1.000- |
| 127.368 | 5.560 | 4.250 | 4.256- | 46.415 | 8.500 | 1.000- |
| 131.102 | 5.620 | 4.375 | 4.381- | 46.915 | 8.750 | 1.000- |
| 134.856 | 5.775 | 4.501 | 4.506- | 48.209 | 9.002 | 1.000- |
| 138.59 | 5.980 | 4.625 | 4.630- | 49.921 | 9.250 | 1.000- |
| 142.344 | 6.190 | 4.750 | 4.756- | 51.674 | 9.500 | 1.000- |
| 146.077 | 6.485 | 4.875 | 4.880- | 54.136 | 9.750 | 1.000- |
| 149.831 | 6.765 | 5.000 | 5.006- | 56.474 | 10.000 | 1.000- |
| 153.565 | 7.005 | 5.125 | 5.130- | 58.477 | 10.250 | 1.000- |
| 157.299 | 7.155 | 5.250 | 5.256- | 59.730 | 10.500 | 1.000- |
| 161.013 | 7.265 | 5.375 | 5.380- | 60.648 | 10.750 | 1.000- |
| 164.727 | 7.295 | 5.500 | 5.506- | 60.898 | 11.000 | 1.000- |
| 168.44 | 7.480 | 5.625 | 5.630- | 62.443 | 11.250 | 1.000- |
| 172.174 | 7.725 | 5.750 | 5.756- | 64.488 | 11.500 | 1.000- |
| 175.888 | 7.930 | 5.875 | 5.880- | 66.199 | 11.750 | 1.000- |
| 179.602 | 8.195 | 6.000 | 6.006- | 68.411 | 12.000 | 1.000- |
| 183.336 | 8.400 | 6.125 | 6.130- | 70.123 | 12.250 | 1.000- |
| 187.05 | 8.590 | 6.250 | 6.256- | 71.709 | 12.500 | 1.000- |
| 189.405 | 8.675 | 6.329 | 6.334- | 72.418 | 12.658 | 1.000- |

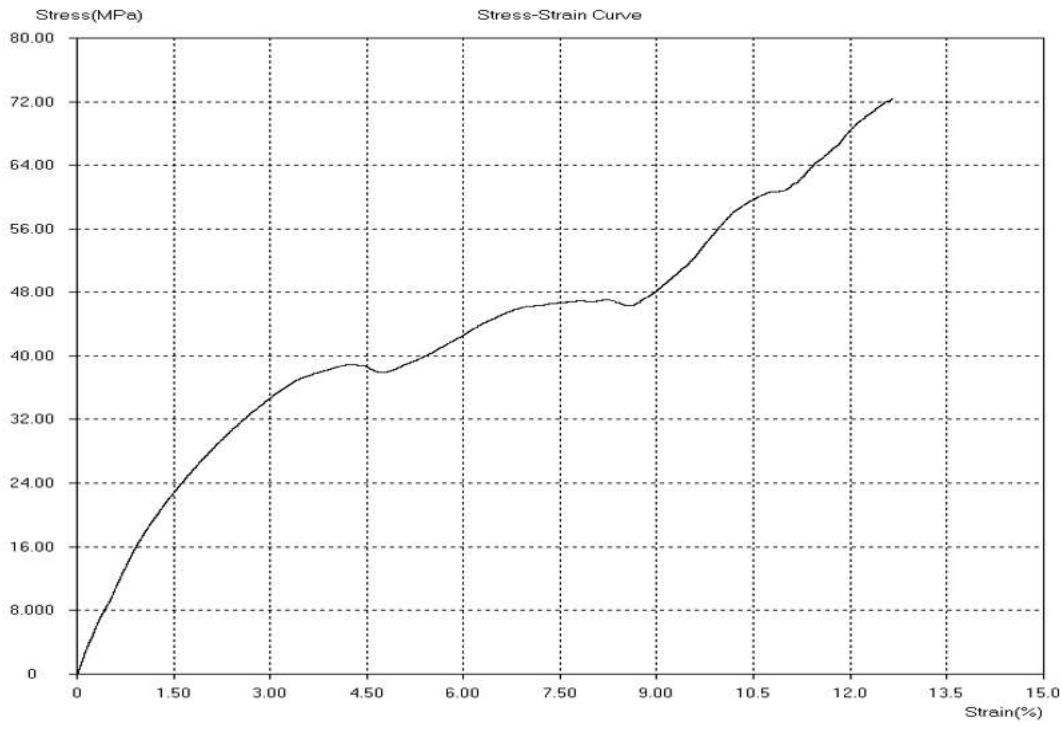


**Figure 4.8** Compressive strength (Stress Strain Curve) for Specimen 2

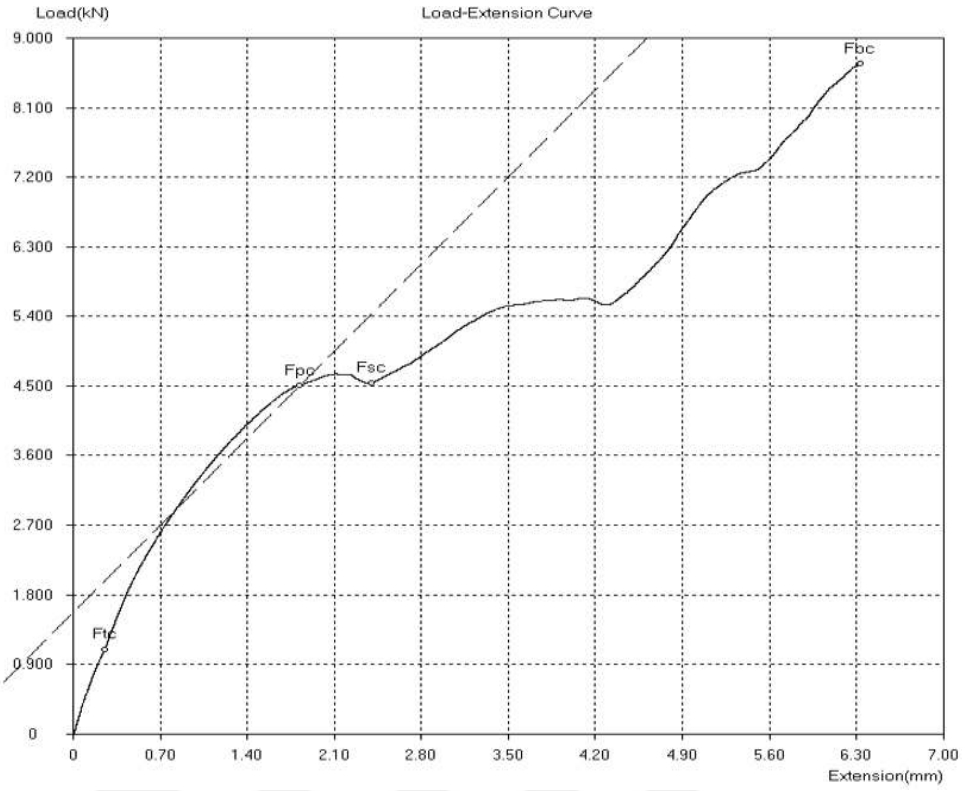


**Figure 4.9** Compressive strength (Load Extension Curve) for Specimen 2

**Table 4.7** Compressive strength values (Stress Strain Curve) for Specimen 3

| **S3NO** | | | **SampleID** | | | |
|---|---|---|---|---|---|---|
| 1.04.2022 | | | TestDate | | | |
| S3NO | | | Operator | | | |
| Circle | | | Type | | | |
| 10 | | | Size(mm) | | | |
| 13.94 | | | Fbc(kN) | | | |
| 116 | | | Rbc(MPa) | | | |
| 0.81 | | | Ftc(kN) | | | |
| 7 | | | Rtc(MPa) | | | |
| 0.64 | | | Ec(GPa) | | | |
| ----------Curve---------- | | | | | | |
| **Time** | **Load** | **Elong** | **Displacement** | **Stress** | **Strain** | **Width** |
| 0 | 0.000 | 0.000 | 0.003- | 0.000 | 0.000 | 0.000 |
| 0 | 0.000 | 0.003- | 0.000 | 0.000 | 0.006- | 1.000- |
| 3.873 | 0.390 | 0.125 | 0.127- | 3.256 | 0.250 | 1.000- |
| 7.627 | 0.810 | 0.250 | 0.253- | 6.762 | 0.500 | 1.000- |
| Kas.34 | 1.220 | 0.375 | 0.377- | 10.184 | 0.750 | 1.000- |
| 15.094 | 1.550 | 0.500 | 0.503- | 12.939 | 1.000 | 1.000- |
| 18.808 | 1.850 | 0.625 | 0.628- | 15.444 | 1.250 | 1.000- |
| 22.522 | 2.115 | 0.750 | 0.753- | 17.656 | 1.500 | 1.000- |
| 26.236 | 2.365 | 0.875 | 0.877- | 19.743 | 1.750 | 1.000- |

**Table 4.7** Compressive strength values (Stress Strain Curve) for Specimen 3 (Continued)

| Time | Load | Elong | Displacement | Stress | Strain | Width |
|---|---|---|---|---|---|---|
| 29.969 | 2.605 | 1.000 | 1.003- | 21.746 | 2.000 | 1.000- |
| 33.664 | 2.830 | 1.125 | 1.127- | 23.625 | 2.250 | 1.000- |
| 37.397 | 3.050 | 1.250 | 1.253- | 25.461 | 2.500 | 1.000- |
| 41.111 | 3.265 | 1.375 | 1.377- | 27.256 | 2.750 | 1.000- |
| 41.131 | 3.265 | 1.375 | 1.378- | 27.256 | 2.750 | 1.000- |
| 44.865 | 3.470 | 1.500 | 1.503- | 28.967 | 3.000 | 1.000- |
| 48.579 | 3.675 | 1.625 | 1.627- | 30.679 | 3.250 | 1.000- |
| 52.333 | 3.870 | 1.750 | 1.753- | 32.307 | 3.500 | 1.000- |
| 56.066 | 4.065 | 1.875 | 1.877- | 33.934 | 3.750 | 1.000- |
| 59.799 | 4.255 | 2.000 | 2.003- | 35.520 | 4.000 | 1.000- |
| 63.513 | 4.445 | 2.125 | 2.127- | 37.107 | 4.250 | 1.000- |
| 67.267 | 4.640 | 2.251 | 2.253- | 38.734 | 4.502 | 1.000- |
| 70.981 | 4.825 | 2.375 | 2.377- | 40.279 | 4.750 | 1.000- |
| 74.715 | 5.010 | 2.500 | 2.503- | 41.823 | 5.000 | 1.000- |
| 78.449 | 5.195 | 2.625 | 2.627- | 43.368 | 5.250 | 1.000- |
| 82.182 | 5.385 | 2.750 | 2.753- | 44.954 | 5.500 | 1.000- |
| 85.917 | 5.575 | 2.875 | 2.877- | 46.540 | 5.750 | 1.000- |
| 89.671 | 5.770 | 3.000 | 3.003- | 48.168 | 6.000 | 1.000- |
| 93.424 | 5.965 | 3.125 | 3.127- | 49.795 | 6.250 | 1.000- |
| 97.198 | 6.155 | 3.251 | 3.253- | 51.382 | 6.502 | 1.000- |
| 100.971 | 6.340 | 3.375 | 3.378- | 52.926 | 6.750 | 1.000- |
| 104.706 | 6.530 | 3.500 | 3.503- | 54.512 | 7.000 | 1.000- |
| 108.459 | 6.725 | 3.625 | 3.627- | 56.140 | 7.250 | 1.000- |
| 112.233 | 6.940 | 3.750 | 3.753- | 57.935 | 7.500 | 1.000- |
| 115.966 | 7.155 | 3.875 | 3.877- | 59.730 | 7.750 | 1.000- |
| 119.72 | 7.395 | 4.000 | 4.003- | 61.733 | 8.000 | 1.000- |
| 123.454 | 7.640 | 4.125 | 4.127- | 63.778 | 8.250 | 1.000- |
| 127.208 | 7.880 | 4.250 | 4.253- | 65.782 | 8.500 | 1.000- |
| 130.942 | 8.125 | 4.375 | 4.377- | 67.827 | 8.750 | 1.000- |
| 134.696 | 8.360 | 4.500 | 4.503- | 69.789 | 9.000 | 1.000- |
| 138.449 | 8.585 | 4.625 | 4.627- | 71.667 | 9.250 | 1.000- |
| 142.203 | 8.800 | 4.750 | 4.753- | 73.462 | 9.500 | 1.000- |
| 145.937 | 8.955 | 4.875 | 4.877- | 74.756 | 9.750 | 1.000- |
| 149.691 | 9.075 | 5.001 | 5.003- | 75.758 | 10.002 | 1.000- |
| 153.384 | 9.220 | 5.125 | 5.127- | 76.968 | 10.250 | 1.000- |
| 157.138 | 9.455 | 5.250 | 5.253- | 78.930 | 10.500 | 1.000- |
| 160.832 | 9.750 | 5.375 | 5.377- | 81.392 | 10.750 | 1.000- |
| 164.566 | 10.070 | 5.500 | 5.503- | 84.064 | 11.000 | 1.000- |
| 168.28 | 10.390 | 5.625 | 5.627- | 86.735 | 11.250 | 1.000- |
| 172.013 | 10.760 | 5.750 | 5.753- | 89.824 | 11.500 | 1.000- |
| 175.708 | 11.150 | 5.875 | 5.877- | 93.080 | 11.750 | 1.000- |
| 179.462 | 11.580 | 6.000 | 6.003- | 96.669 | 12.000 | 1.000- |
| 183.175 | 12.050 | 6.125 | 6.128- | 100.593 | 12.250 | 1.000- |
| 186.909 | 12.520 | 6.250 | 6.253- | 104.516 | 12.500 | 1.000- |

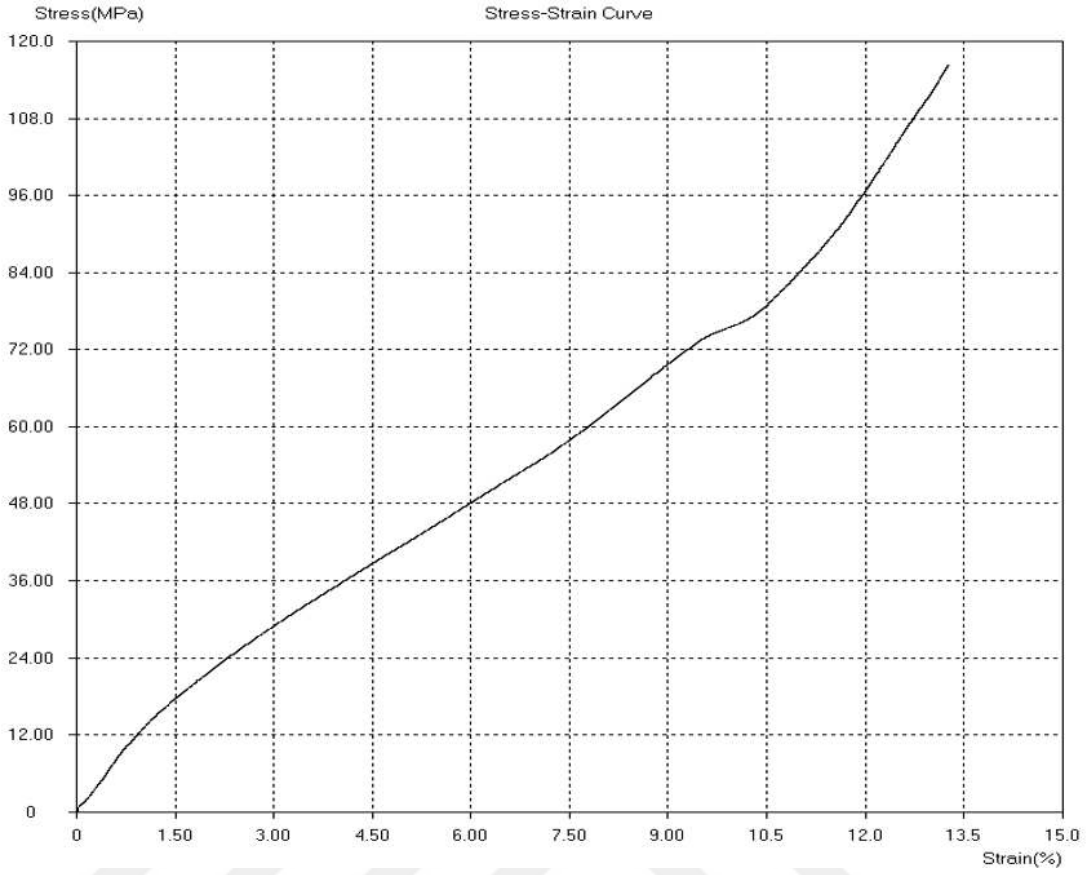


**Figure 4.10** Compressive strength (Stress Strain Curve) for Specimen 3

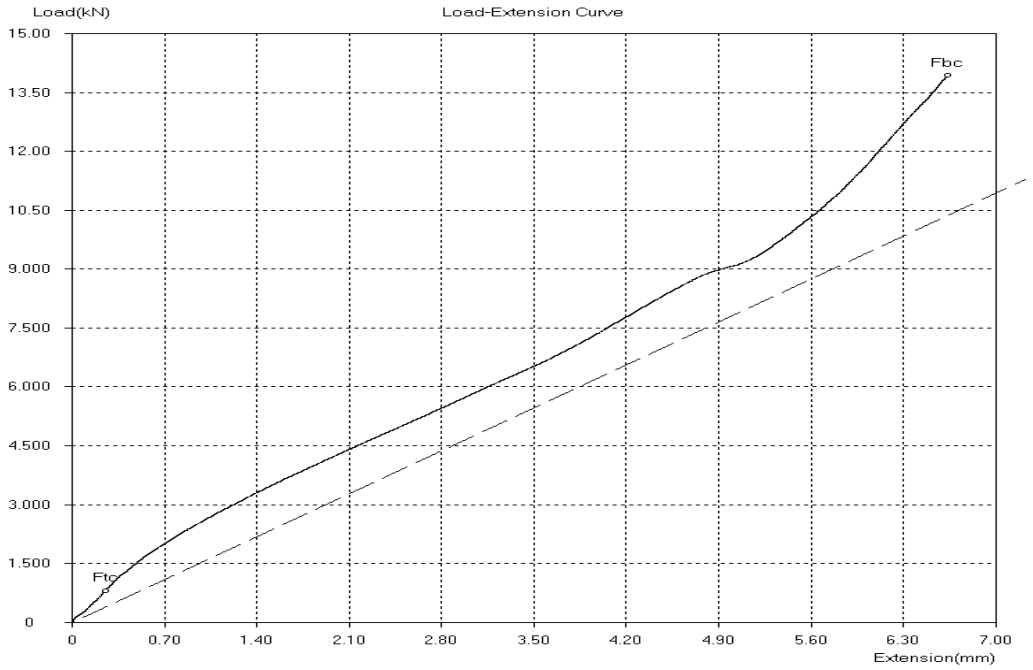


**Figure 4.11** Compressive strength (Load Extension Curve) for Specimen 3

**Table 4.8** Compressive strength values (Stress Strain Curve) for Specimen 4

| **S4NO** | **SampleID** |
|---|---|
| 1.04.2022 | TestDate |
| S4NO | Operator |
| Circle | Type |
| 10 | Size(mm) |
| 9.73 | Fbc(kN) |
| 81 | Rbc(MPa) |
| 8.06 | Fsc(kN) |
| 67 | Rsc(MPa) |
| 0.80 | Ftc(kN) |
| 7 | Rtc(MPa) |
| 0.53 | Ec(GPa) |

----------Curve----------

| **Time** | **Load** | **Elong** | **Displacement** | **Stress** | **Strain** | **Width** |
|---|---|---|---|---|---|---|
| 0 | 0.000 | 0.000 | 0.000 | 0.000 | 0.000 | 0.000 |
| 0 | 0.000 | 0.004- | 0.000 | 0.000 | 0.008- | 1.000- |
| 4.013 | 0.330 | 0.125 | 0.129- | 2.755 | 0.250 | 1.000- |
| 7.767 | 0.795 | 0.250 | 0.254- | 6.637 | 0.500 | 1.000- |
| .11May | 1.270 | 0.375 | 0.379- | 10.602 | 0.750 | 1.000- |
| 15.234 | 1.625 | 0.500 | 0.504- | 13.565 | 1.000 | 1.000- |
| 18.948 | 1.955 | 0.625 | 0.629- | 16.320 | 1.250 | 1.000- |
| 22.682 | 2.240 | 0.750 | 0.754- | 18.699 | 1.500 | 1.000- |
| 26.395 | 2.495 | 0.875 | 0.879- | 20.828 | 1.750 | 1.000- |
| 30.13 | 2.735 | 1.000 | 1.004- | 22.832 | 2.000 | 1.000- |
| 33.844 | 2.960 | 1.125 | 1.129- | 24.710 | 2.250 | 1.000- |
| 37.558 | 3.175 | 1.250 | 1.254- | 26.505 | 2.500 | 1.000- |
| 41.27 | 3.375 | 1.375 | 1.379- | 28.174 | 2.750 | 1.000- |
| 45.005 | 3.565 | 1.500 | 1.504- | 29.760 | 3.000 | 1.000- |
| 48.719 | 3.750 | 1.625 | 1.629- | 31.305 | 3.250 | 1.000- |
| 52.473 | 3.930 | 1.750 | 1.754- | 32.807 | 3.500 | 1.000- |
| 56.186 | 4.105 | 1.875 | 1.879- | 34.268 | 3.750 | 1.000- |
| 59.94 | 4.275 | 2.000 | 2.004- | 35.687 | 4.000 | 1.000- |
| 63.654 | 4.440 | 2.125 | 2.129- | 37.065 | 4.250 | 1.000- |
| 67.388 | 4.590 | 2.250 | 2.254- | 38.317 | 4.500 | 1.000- |
| 71.121 | 4.740 | 2.375 | 2.379- | 39.569 | 4.750 | 1.000- |
| 74.855 | 4.880 | 2.500 | 2.504- | 40.738 | 5.000 | 1.000- |
| 78.569 | 5.020 | 2.625 | 2.629- | 41.907 | 5.250 | 1.000- |
| 82.323 | 5.170 | 2.750 | 2.754- | 43.159 | 5.500 | 1.000- |
| 86.037 | 5.325 | 2.875 | 2.879- | 44.453 | 5.750 | 1.000- |
| 89.79 | 5.485 | 3.000 | 3.004- | 45.788 | 6.000 | 1.000- |
| 93.524 | 5.640 | 3.125 | 3.129- | 47.082 | 6.250 | 1.000- |
| 97.278 | 5.800 | 3.250 | 3.254- | 48.418 | 6.500 | 1.000- |
| 101.031 | 5.955 | 3.375 | 3.379- | 49.712 | 6.750 | 1.000- |
| 104.785 | 6.125 | 3.500 | 3.504- | 51.131 | 7.000 | 1.000- |
| 108.56 | 6.315 | 3.625 | 3.629- | 52.717 | 7.250 | 1.000- |
| 112.312 | 6.530 | 3.750 | 3.754- | 54.512 | 7.500 | 1.000- |
| 116.066 | 6.740 | 3.875 | 3.879- | 56.265 | 7.750 | 1.000- |
| 119.82 | 6.955 | 4.000 | 4.004- | 58.060 | 8.000 | 1.000- |
| 123.574 | 7.175 | 4.125 | 4.130- | 59.896 | 8.250 | 1.000- |
| 127.308 | 7.390 | 4.250 | 4.254- | 61.691 | 8.500 | 1.000- |
| 131.061 | 7.600 | 4.375 | 4.379- | 63.444 | 8.750 | 1.000- |

**Table 4.8** Compressive strength values (Stress Strain Curve) for Specimen 4 (Continued)

| Time | Load | Elong | Displacement | Stress | Strain | Width |
|---|---|---|---|---|---|---|
| 134.796 | 7.815 | 4.500 | 4.504- | 65.239 | 9.000 | 1.000- |
| 138.55 | 7.990 | 4.625 | 4.629- | 66.700 | 9.250 | 1.000- |
| 142.283 | 8.115 | 4.750 | 4.754- | 67.744 | 9.500 | 1.000- |
| 146.037 | 8.125 | 4.875 | 4.879- | 67.827 | 9.750 | 1.000- |
| 149.77 | 8.080 | 5.000 | 5.004- | 67.451 | 10.000 | 1.000- |
| 153.524 | 8.175 | 5.125 | 5.129- | 68.244 | 10.250 | 1.000- |
| 157.259 | 8.375 | 5.250 | 5.254- | 69.914 | 10.500 | 1.000- |
| 160.972 | 8.595 | 5.375 | 5.379- | 71.751 | 10.750 | 1.000- |
| 164.706 | 8.815 | 5.500 | 5.504- | 73.587 | 11.000 | 1.000- |
| 168.421 | 9.020 | 5.625 | 5.629- | 75.298 | 11.250 | 1.000- |
| 172.134 | 9.210 | 5.750 | 5.754- | 76.885 | 11.500 | 1.000- |
| 175.848 | 9.455 | 5.875 | 5.879- | 78.930 | 11.750 | 1.000- |
| 179.581 | 9.685 | 6.000 | 6.004- | 80.850 | 12.000 | 1.000- |
| 180.579 | 9.735 | 6.034 | 6.038- | 81.267 | 12.068 | 1.000- |

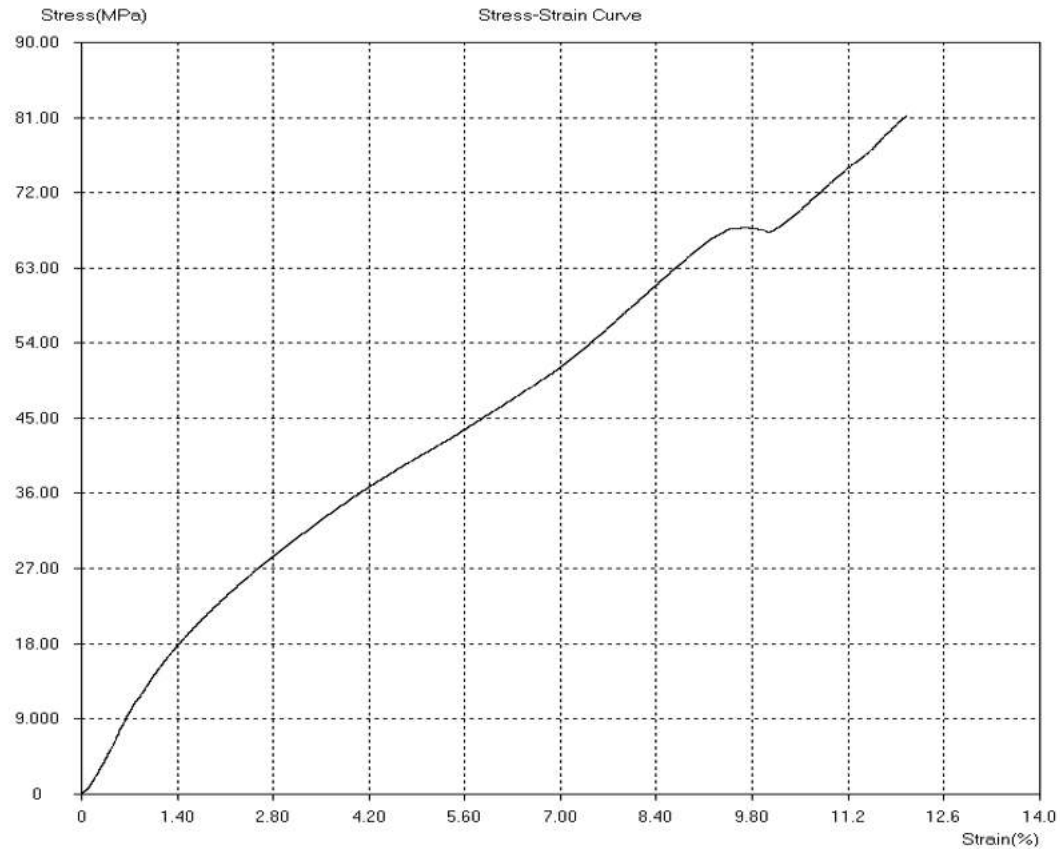


**Figure 4.12** Compressive strength (Stress Strain Curve) for Specimen 4

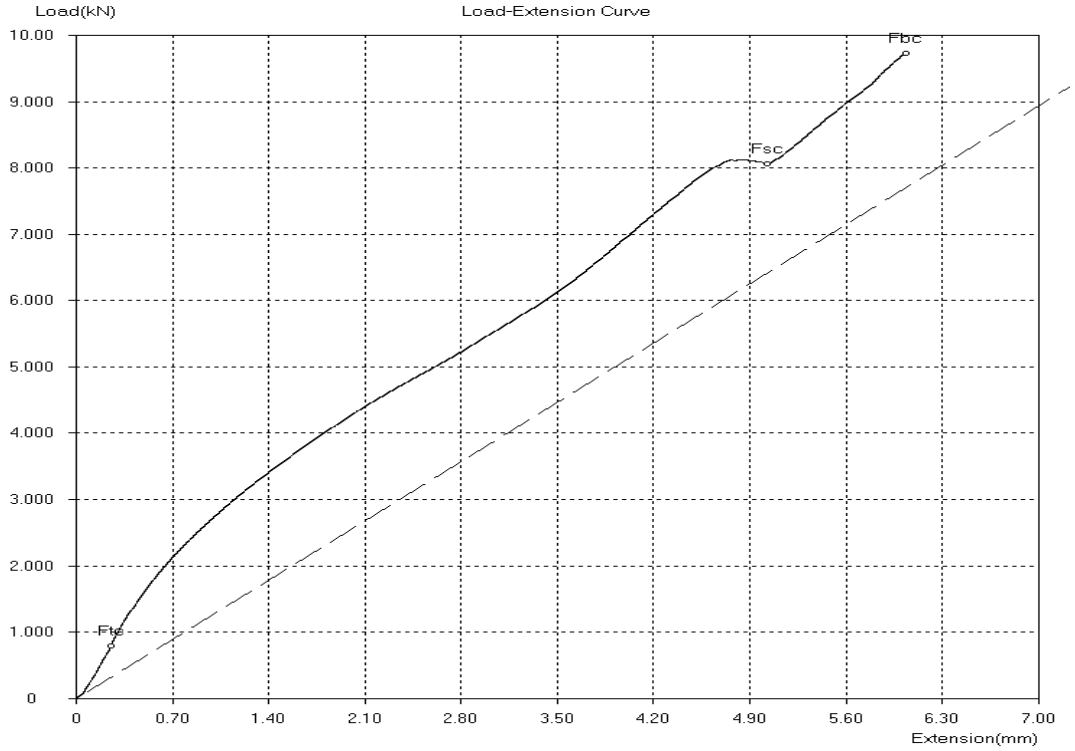


**Figure 4.13** Compressive strength (Load Extension Curve) for Specimen 4

**Table 4.9** Compressive strength values (Stress Strain Curve) for Specimen 5

| **S5NO** | **SampleID** |
|---|---|
| 1.04.2022 | TestDate |
| S5NO | Operator |
| Circle | Type |
| 10 | Size(mm) |
| 15.70 | Fbc(kN) |
| 131 | Rbc(MPa) |
| .1Şub | Ftc(kN) |
| 9 | Rtc(MPa) |
| 0.91 | Ec(GPa) |

----------Curve----------

| **Time** | **Load** | **Elong** | **Displacement** | **Stress** | **Strain** | **Width** |
|---|---|---|---|---|---|---|
| 0 | 0.000 | 0.000 | 0.001- | 0.000 | 0.000 | 0.000 |
| 0 | 0.000 | 0.006 | 0.000 | 0.000 | 0.012- | 1.000- |
| 4.014 | 0.420 | 0.125 | 0.131- | 3.506 | 0.250 | 1.000- |
| 7.767 | 1.020 | 0.250 | 0.256- | 8.515 | 0.500 | 1.000- |
| 11.481 | 1.450 | 0.375 | 0.381- | 12.105 | 0.750 | 1.000- |
| 15.215 | 1.815 | 0.500 | 0.506- | 15.152 | 1.000 | 1.000- |
| 18.929 | 2.110 | 0.625 | 0.631- | 17.614 | 1.250 | 1.000- |
| 22.643 | 2.390 | 0.750 | 0.756- | 19.952 | 1.500 | 1.000- |
| 26.357 | 2.660 | 0.875 | 0.881- | 22.206 | 1.750 | 1.000- |
| 30.071 | 2.920 | 1.000 | 1.006- | 24.376 | 2.000 | 1.000- |
| 33.785 | 3.175 | 1.125 | 1.131- | 26.505 | 2.250 | 1.000- |
| 37.518 | 3.430 | 1.250 | 1.256- | 28.633 | 2.500 | 1.000- |

**Table 4.9** Compressive strength values (Stress Strain Curve) for Specimen 5 (Continued)

| Time | Load | Elong | Displacement | Stress | Strain | Width |
|---|---|---|---|---|---|---|
| 41.212 | 3.670 | 1.375 | 1.381- | 30.637 | 2.750 | 1.000- |
| 44.965 | 3.915 | 1.500 | 1.506- | 32.682 | 3.000 | 1.000- |
| 48.679 | 4.150 | 1.625 | 1.631- | 34.644 | 3.250 | 1.000- |
| 52.433 | 4.380 | 1.750 | 1.756- | 36.564 | 3.500 | 1.000- |
| 56.148 | 4.615 | 1.875 | 1.881- | 38.526 | 3.750 | 1.000- |
| 59.901 | 4.850 | 2.000 | 2.006- | 40.488 | 4.000 | 1.000- |
| 63.615 | 5.085 | 2.125 | 2.131- | 42.449 | 4.250 | 1.000- |
| 67.348 | 5.315 | 2.250 | 2.256- | 44.369 | 4.500 | 1.000- |
| 71.062 | 5.555 | 2.375 | 2.381- | 46.373 | 4.750 | 1.000- |
| 74.796 | 5.795 | 2.500 | 2.506- | 48.376 | 5.000 | 1.000- |
| 78.51 | 6.030 | 2.625 | 2.631- | 50.338 | 5.250 | 1.000- |
| 82.264 | 6.280 | 2.750 | 2.756- | 52.425 | 5.500 | 1.000- |
| 85.997 | 6.530 | 2.875 | 2.881- | 54.512 | 5.750 | 1.000- |
| 89.751 | 6.790 | 3.000 | 3.006- | 56.683 | 6.000 | 1.000- |
| 93.505 | 7.060 | 3.125 | 3.131- | 58.936 | 6.250 | 1.000- |
| 97.259 | 7.335 | 3.250 | 3.256- | 61.232 | 6.500 | 1.000- |
| 101.012 | 7.625 | 3.375 | 3.381- | 63.653 | 6.750 | 1.000- |
| 104.787 | 7.920 | 3.500 | 3.506- | 66.116 | 7.000 | 1.000- |
| 108.54 | 8.230 | 3.625 | 3.631- | 68.704 | 7.250 | 1.000- |
| 112.294 | 8.550 | 3.750 | 3.756- | 71.375 | 7.500 | 1.000- |
| 116.028 | 8.880 | 3.875 | 3.881- | 74.130 | 7.750 | 1.000- |
| 119.782 | 9.215 | 4.000 | 4.006- | 76.926 | 8.000 | 1.000- |
| 123.515 | 9.570 | 4.125 | 4.131- | 79.890 | 8.250 | 1.000- |
| 127.269 | 9.935 | 4.250 | 4.256- | 82.937 | 8.500 | 1.000- |
| 131.023 | 10.310 | 4.375 | 4.381- | 86.067 | 8.750 | 1.000- |
| 134.777 | 10.710 | 4.500 | 4.506- | 89.406 | 9.000 | 1.000- |
| 138.51 | 11.110 | 4.625 | 4.631- | 92.746 | 9.250 | 1.000- |
| 142.264 | 11.530 | 4.750 | 4.756- | 96.252 | 9.500 | 1.000- |
| 145.997 | 11.960 | 4.875 | 4.881- | 99.841 | 9.750 | 1.000- |
| 149.751 | 12.410 | 5.000 | 5.006- | 103.598 | 10.000 | 1.000- |
| 153.465 | 12.860 | 5.125 | 5.131- | 107.355 | 10.250 | 1.000- |
| 157.2 | 13.330 | 5.250 | 5.256- | 111.278 | 10.500 | 1.000- |
| 160.913 | 13.810 | 5.375 | 5.381- | 115.285 | 10.750 | 1.000- |
| 164.627 | 14.310 | 5.500 | 5.506- | 119.459 | 11.000 | 1.000- |
| 168.341 | 14.820 | 5.625 | 5.631- | 123.717 | 11.250 | 1.000- |
| 172.075 | 15.340 | 5.750 | 5.756- | 128.057 | 11.500 | 1.000- |
| 174.51 | 15.700 | 5.832 | 5.838- | 131.063 | 11.664 | 1.000- |

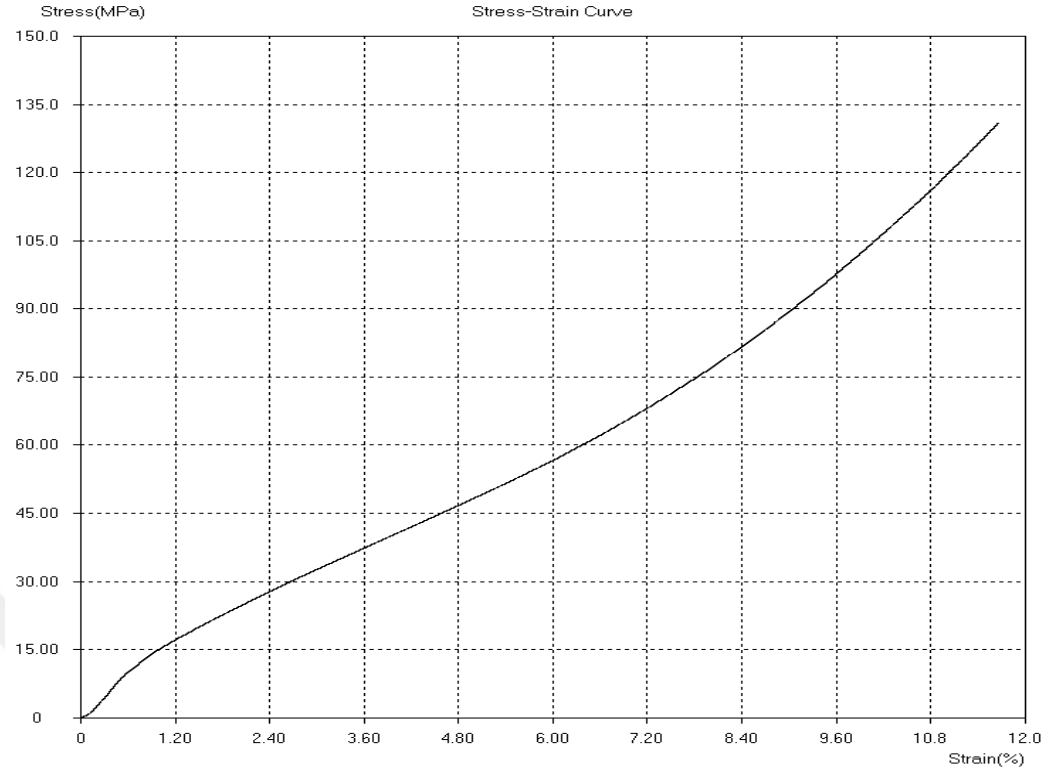


**Figure 4.14** Compressive strength (Stress Strain Curve) for Specimen 5

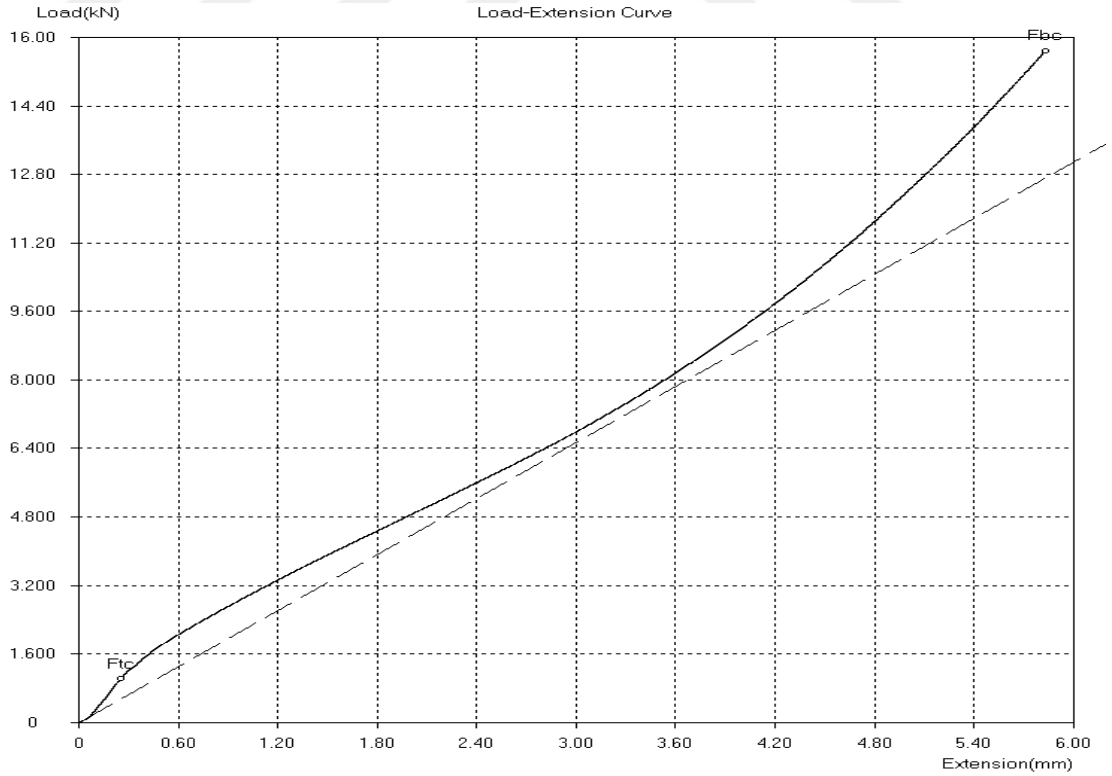


**Figure 4.15** Compressive strength (Load Extension Curve) for Specimen 5

## 4.4 Scanning Electron Microscope Tests (SEM)

The scan was carried out using an electron microscope scanner (SEM) type (Tescan) model (MIRA3) French origin in the State of Iran University of Tehran (Figure 4.16).


**Figure 4.16** Electron microscope scanner (SEM)

This device is distinguished from optical microscopes by using electrons as an alternative to light waves; We get 3D magnifying images in white and black because they depend on light waves.

The surface topography of the Specimen produced after sintering was examined to find out the outsoles of the later Specimen and their coherence. Inside the airless column of an electron microscope, through a sealed facility or dam. The Specimen is then coated with silver or gold, which have an electrical conductivity that promotes electron conduction (Figure 4.17) (Cullity 1956, Karim *et al*. 2021).

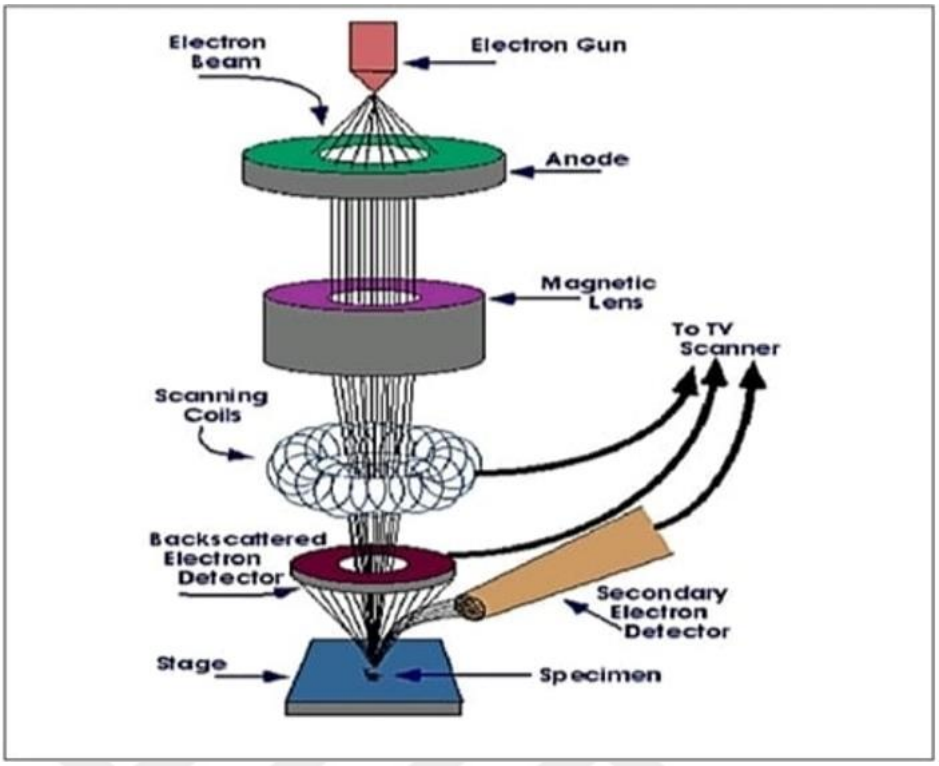


**Figure 4.17** The work of the scanning field emitting electron microscope (Smith and Oatley 1955)

## 4.5 Energy-Dispersive/X-Ray Spectroscopy

Also known as EDS or EDX is an analytical method used to evaluate a specimen's chemical components or determine its elemental composition. It is one of the X-ray fluorescence spectroscopy types that examines patterns through interactions between electromagnetic radiation and matter by examining X-rays of being struck by charged particles.

## 4.6 X-Ray Diffraction (XRD)

In this scan, a type device used is X Pert high score plus dutch origin in Kashan University in Iran, and the used tube (Cu) Kα

The tests at room temperature and Table 4.10 showed the device specifications when the values of the inter-distances of the D levels were known for each specimen and obtained by comparing the values of the inter-distance (d).

**Table 4.10** XRD test conditions

| **Voltage** | **40 KV** |
|---|---|
| Current | 30 mA |
| Wavelength | 1.54060 Å |
| Scan Range | $5^{o}$–$80^{o}$ |
| Scan Speed | $5^{o}$/min |

The intensity of the scans and the angle according to the special standard shapes and tables, through which we obtain Miller coefficients to determine the arrangement of the atoms. When the X-ray falls on the atoms of the material to be measured, the X-ray beam is converted to different directions and based on the intensity and angle of the deviation. X-rays are produced in the X-ray tube by using the electrons colliding with the goal's steel. The English scientist (W.L. Bragg) discovered a mathematical equation to discover the space between the crystal degrees through the usage of x-ray beams (Figure 4.18) (Figure 4.19) (Figure 4.20) (Figure 4.21) (Figure 4.22).

This equation is based on the fact that atoms inside the ballast are lined up in distinct groups of levels. When a pack of X-rays falls at these levels, they are asked in all directions within the crystal where the type of material formed within the material can be defined using in Equation (4.4) (Singh *et al*. 2012, Salih *et al*. 2021).

$$2d \sin\theta = \lambda n \qquad (4.4)$$

- d: Distance between atomic levels
- θ: Diffraction angle
- λ: Wavelength
- n: diffraction peak (integer no)

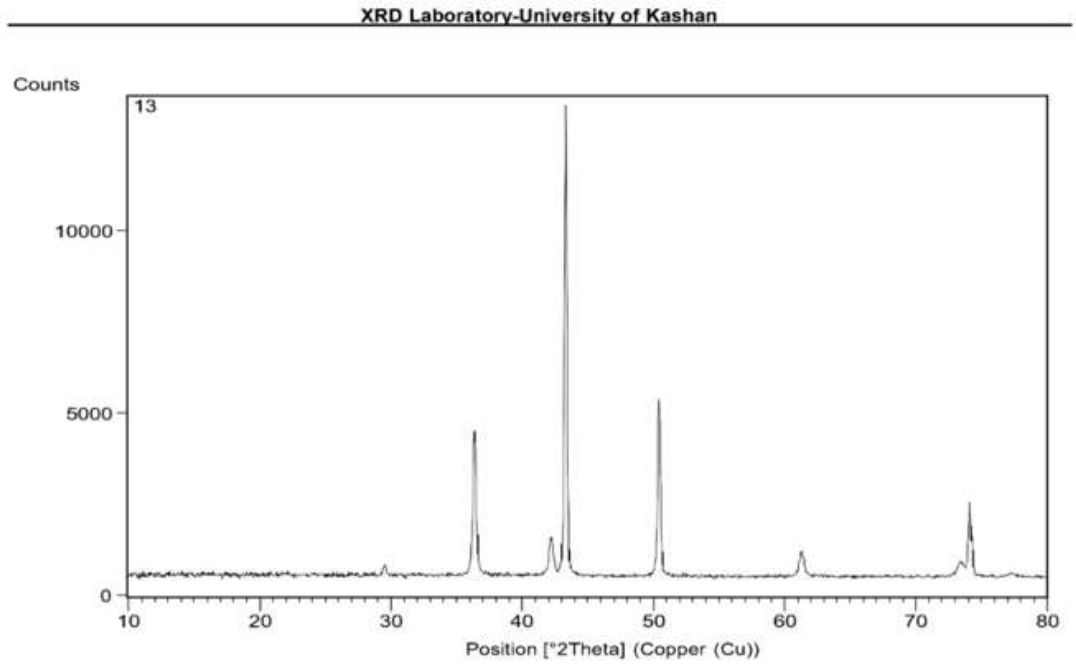


**Figure 4.18** X-Ray diffraction of Cu-MgO nano at support ratios of 2% MgO nano and 98% Cu

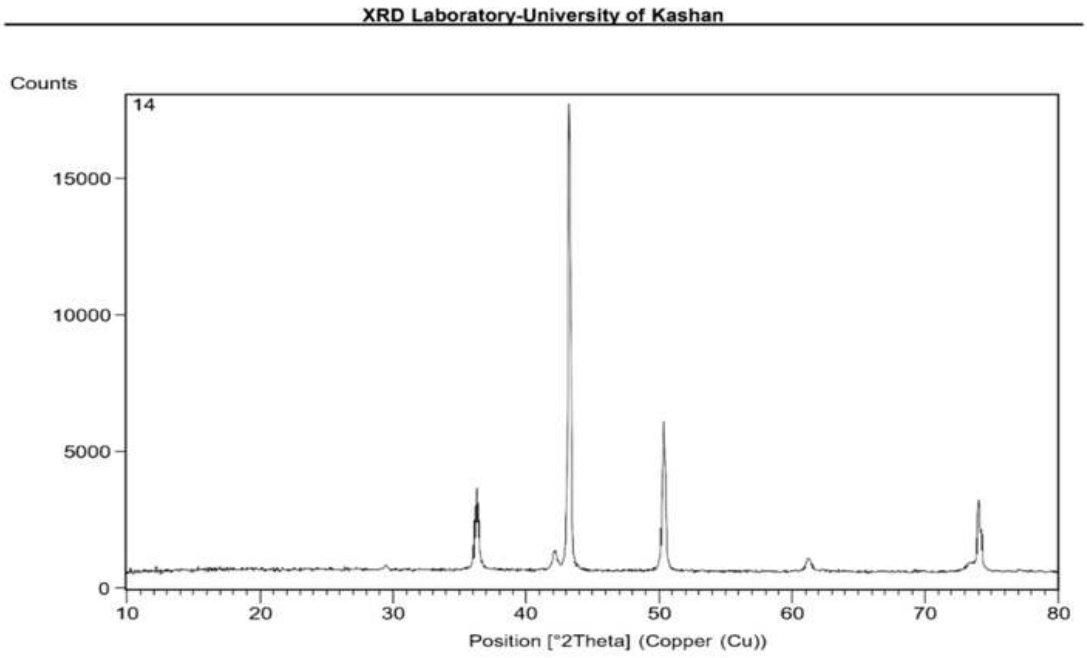


**Figure 4.19** X-Ray diffraction of Cu-MgO nano at support ratios of 4% MgO nano and 96% Cu

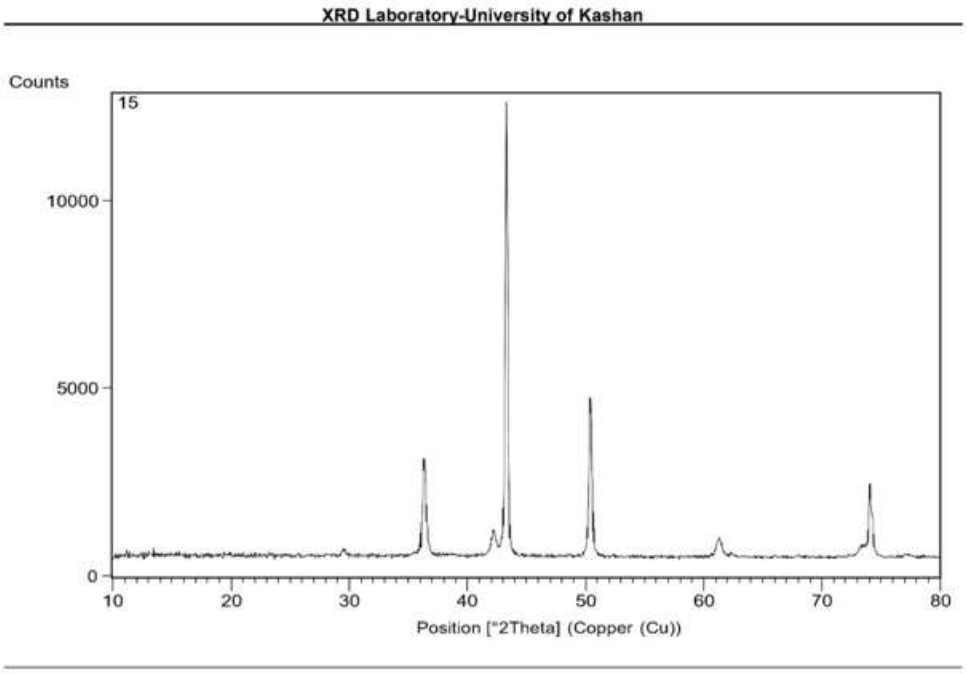


**Figure 4.20** X-Ray diffraction of Cu-MgO nano at support ratios of 6% MgO nano and 94% Cu

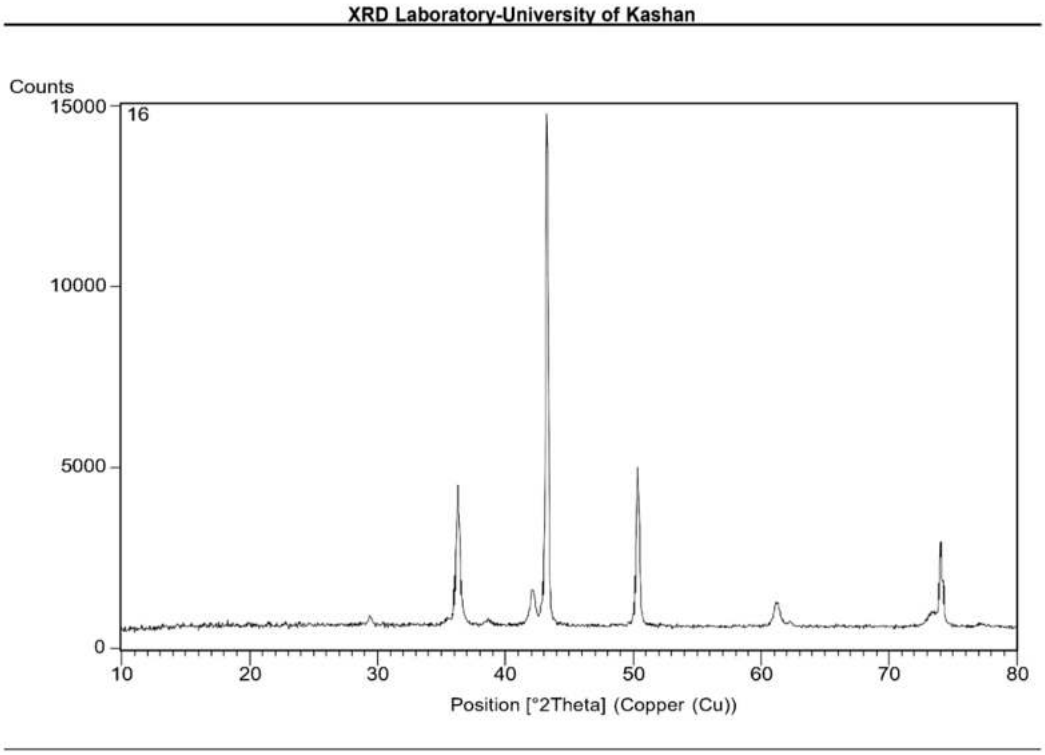


**Figure 4.21** X-Ray diffraction of Cu-MgO nano at support ratios of 8% MgO nano and 92% Cu

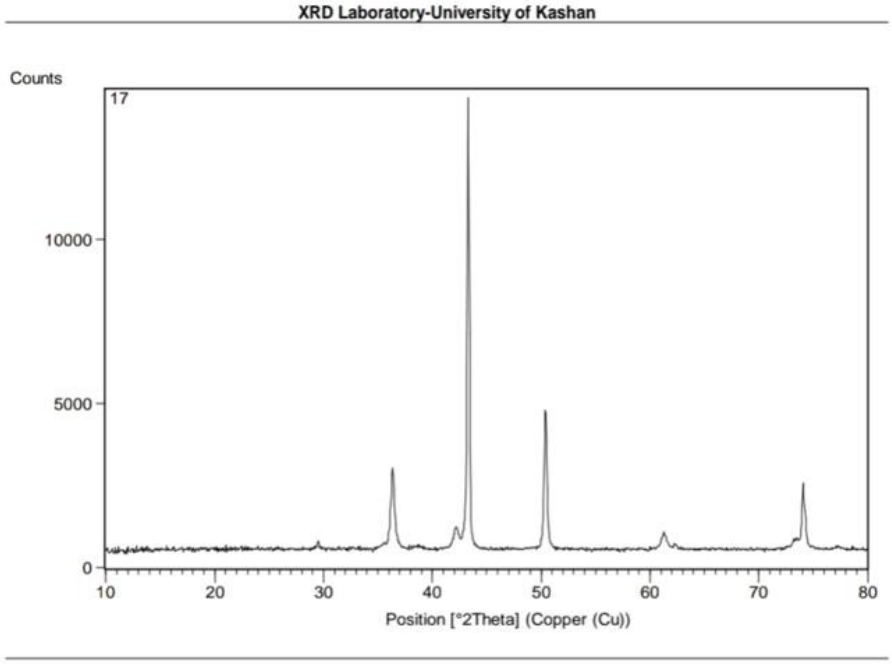


**Figure 4.22** X-Ray diffraction of Cu-MgO nano at support ratios of 10% MgO nano and 90% Cu

Apparent Density, Volumetric Density, Apparent Porosity, True Porosity, Water Absorption Ability

These tests were carried out using the archimedes principle and using a device radwag Wagi elektroniczne model: PS/360/C/1 poland origin sensitive electric balance (Figure 4.23).

**Figure 4.23** Sensitive electric balance

## 4.7 Apparent Density

The apparent density of the density meter was calculated in step with the Archimedes rule and according to the following in Equation (4.5).

$$\rho_a=(W_a/(W_d-W_i)) \times \rho_w \quad (4.5)$$

So that:

- $\rho a$ = Apparent density ($g/cm^3$)
- $\rho w$ = Water density ($g/cm^3$)
- Wd = Body weight is dry (g)
- Wi = Body weight suspended with water (g) (Table 4.11)

**Table 4.11** Apparent density test results before and after sintering process

| MgO % | Apparent density before sintering | Apparent density after sintering |
|---|---|---|
| 2 | 7.77 | 8.001 |
| 4 | 7.34 | 7.67 |
| 6 | 7.22 | 7.53 |
| 8 | 6.95 | 7.33 |
| 10 | 6.71 | 7.11 |
| Grinding Time | 2 h | |

## 4.8 Volumetric Density

Represents the ratio among the mass of the material to its total length, which consists of the actual material and the closed and open pores, Volumetric density may be calculated in step with Archimedes principle through the subsequent Equation (4.6).

$$\rho_b=(W_d/(W_s-W_i))x\rho_w \quad (4.6)$$

- $\rho_b$ = Volumetric density (g/cm$^3$)
- $\rho_w$ = Water density (g/cm$^3$)
- $W_d$ = Dry weight (g)
- Ws = Body weight is saturated with water (g) (Table 4.12)

**Table 4.12** Volumetric density test results before and after sintering process

| MgO % | Volumetric Density before sintering | Volumetric Density after sintering |
|---|---|---|
| 2 | 8.33 | 8.85 |
| 4 | 8.12 | 8.74 |
| 6 | 7.56 | 8.44 |
| 8 | 7.21 | 8.11 |
| 10 | 7.01 | 7.91 |
| Grinding Time | 2 h | |

## 4.9 Apparent Porosity

Apparent Porosity, which is the ratio of open pores to the size of the overall body, obvious porosity is calculated using the Archimedes principle from the following Equation (4.7) (Table 4.13).

$$A.P = (W_S-W_d)/(Ws-W_i)x100\% \quad (4.7)$$

**Table 4.13** Apparent porosity test results before and after sintering process

| MgO % | Apparent Porosity before sintering | Apparent Porosity after sintering |
|---|---|---|
| 2 | 14.32 | 7.6 |
| 4 | 15.43 | 9.9 |
| 6 | 17.45 | 12.44 |
| 8 | 19.55 | 14.56 |
| 10 | 21.56 | 18.82 |
| Grinding Time | 2 h | |

## 4.10 True Porosity

True Porosity is the ratio between the scale of open and closed pores to the overall frame length and calculated from the subsequent Equation (4.8).

$$T.P = \frac{T.D - B.D}{T.D} \times 100\% \quad (4.8)$$

- T.D: body density theoretically sintered
- B.D: body density Practical lactobacillus (Table 4.14)

**Table 4.14** True porosity test results before and after sintering process

| MgO % | True Porosity before sintering | True Porosity after sintering |
|---|---|---|
| 2 | 14.34 | 9.98 |
| 4 | 18.07 | 11.23 |
| 6 | 20.07 | 14.56 |
| 8 | 23.36 | 18.09 |
| 10 | 27.01 | 20.25 |
| Grinding Time | 2 h | |

## 4.11 Water Absorption Ability

Water absorption represents the ratio of open pores' size to the mass of depend (Zeynelabdien *et al*. 2021). Water absorption is a function through which the product can be decided, and the product is porous if the water absorption fee is greater than 1%.

Water absorption is directly proportional to porous because the open pores in the material absorb water, and the absorption of water is affected by the same factors that affect pores, such as the granular size of the material and the conditions of formation and sintering (Ramakrishnan 1983).

Water absorption can be calculated in keeping with Archimedes principle from the following in Equation (4.9) (Table 4.15).

$$W.A = ((W_s-W_d)/(W_d)x100\% \quad (4.9)$$

**Table 4.15** Water absorption ability test results before and after sintering process

| MgO % | Water Absorption Ability before sintering | Water Absorption Ability after sintering |
|---|---|---|
| 2 | 0.7 | 0.26 |
| 4 | 0.72 | 0.33 |
| 6 | 0.81 | 0.52 |
| 8 | 0.9 | 0.63 |
| 10 | 0.97 | 0.83 |
| Grinding Time | 2 h | |

## 4.12 Microstracuture Test

After the refinement and softening process, a microscopy of the specimens was performed (Figure 4.24) (Figure 4.25).

**Figure 4.24** Microscope

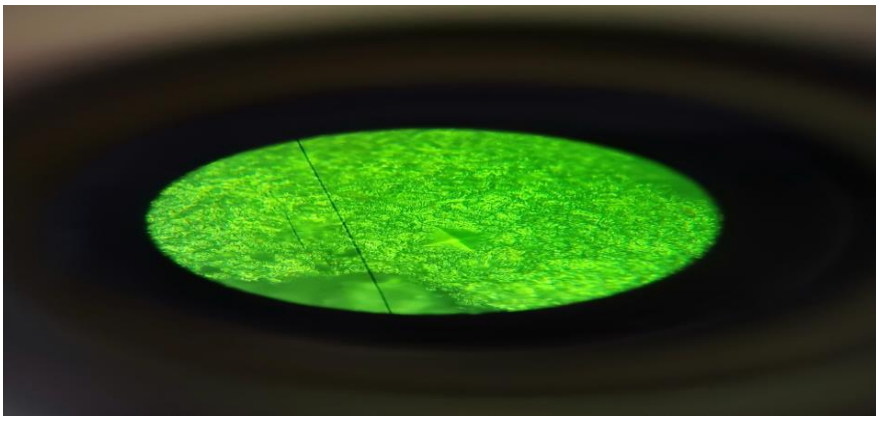

**Figure 4.25** Specimen under microscope

## 4.13 Thermal Conductivity Test

The thermal conductivity test is an Iraqi-made device (Figure 4.26). In this test, the thermal conduction of the specimens was measured after the sintering process (Table 4.16).

**Table 4.16** Thermal conductivity test results

| MgO % | Thermal conductivity before sintering | Thermal conductivity after sintering |
|---|---|---|
| 2 | 296 | 313 |
| 4 | 263 | 276 |
| 6 | 230 | 251 |
| 8 | 211 | 230 |
| 10 | 202 | 218 |
| Grinding Time | 2 h | |

**Figure 4.26** Thermal conductivity device

# 5. RESULTS AND DISCUSSION

## 5.1 Physical Properties

### 5.1.1 Effect of nano MgO strengthening content on water absorption

The relation among the adjustments in the volumetric ratios of nano MgO particle and water absorption before and after the sintering method and we observe from the picture that the increase in the added volumetric ratio of the supporting material nano MgO has led to an increase in water absorption (Figure 5.1).

Pre-sintering water absorption increased from (0.7-0.97) % at nano MgO content of 2-10%. Water absorption after sintering increased from (0.26-0.83) % when the content of nano MgO increased from (2-10)%.

The reason for the increase in water absorption when the content increases nano MgO Both before the sintering and as the apparent decrease in water absorption after the sintering process is from what it was before the sintering of the same volumetric ratios.

However, water absorption depends entirely on the apparent porosity of the overlays, i.e., open porosity, which can be carried out by water inside the overlaps, and the exact causes of Apparent porosity (Yusoff and Hussain 2013, Efe *et al*. 2010).

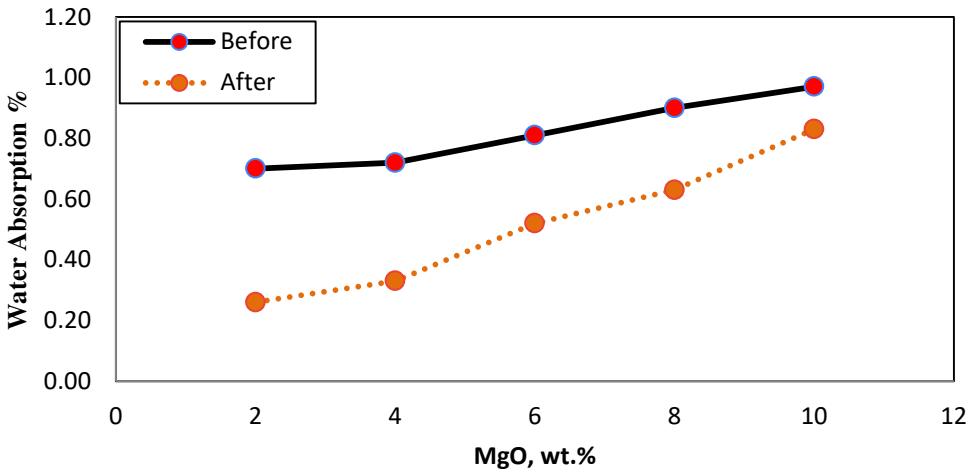


**Figure 5.1** Relation between reinforcement ratios of Cu-MgO nano and water absorption before and after sintering

### 5.1.2 Effect of nano MgO strengthening content on volumetric density

The connection among relation within the volumetric ratios of nano MgO particle and volumetric density before and after the sintering procedure and we note from the picture that the increase in the introduced volumetric ratio of the assisting material nano MgO has led to a decrease. The form suggested the relation between the change in the volumetric ratios of nano MgO particles and the volumetric density after sintering. It decreased from volumetric ratios to 8.85 g/cm$^3$ on the magnesium oxide degree of two percent in which. It became 7.91 g/cm$^3$ at ten percent magnesium oxide, in line with the disk. The cause for this lower volumetric density after sintering to the low density of Nano MgO compared to Cu density is a decrease in volumetric density. We also observe that volumetric density values after sintering have elevated from volumetric density values prior to sintering. The increased bonding strength between Cu and nano MgO due to the temperature of the 900 °C sintering and for a couple of hours, which helped enhance the interface of the overlaps and enhance the bonding among particles (Figure 5.2).

We know that the cold piston method itself consequences in overlays that have green density before the manner of sintering. It is a great deal decrease than the theoretical density, so the volumetric density logically might be higher than the green density and the volumetric density techniques the theoretical density because of the occurrence of the merger among the particles overlapping all through the sintering, which corresponds to what reached (Gan and Gu 2008, Jabur 2013).

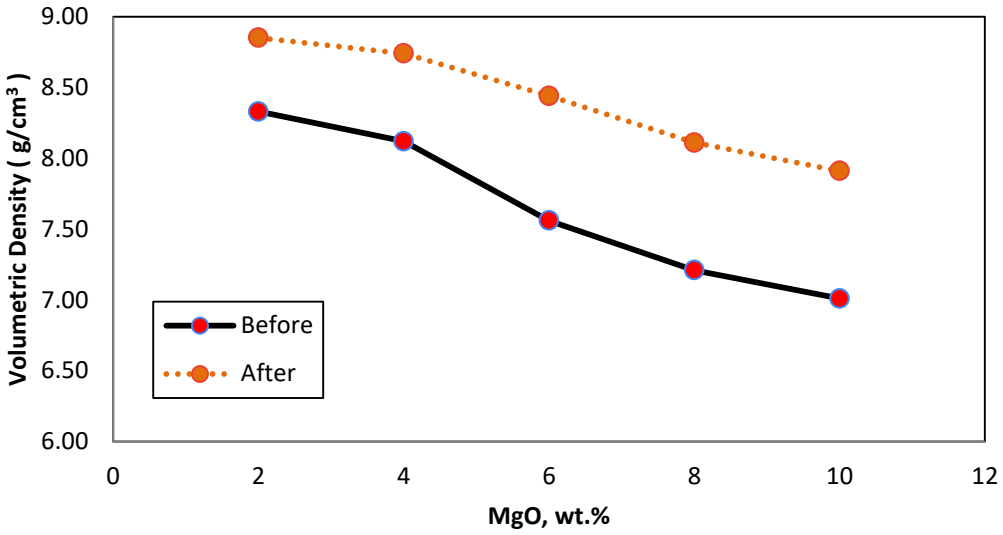


**Figure 5.2** Relation between reinforcement ratios of Cu-MgO nano and volumetric density before and after sintering

### 5.1.3 Effect of nano MgO strengthening content on apparent porosity

The table shows the relationship between changing the volumetric ratio of nano MgO particles and Apparent porosity earlier than and after the sintering system (Figure 5.3).

We note from the figure that the increase in the added volumetric ratio of magnesium oxide nanoscale had led to an increase in apparent porosity before sintering, where it was 14.32 at 2% of nano MgO and then increased sequentially with an increase in nano MgO to 10% where it became 21.56%.

We also note from the figure that the increase in the volumetric ratio of nano MgO after sintering has led to an increase in apparent porosity at the level of nano-Magnesium Oxide 2% was 7.6% where it became at 10% of nano-Magnesium Oxide 18.82.

This is due to the increase in the apparent porous ratio when adding the level of nano-magnesium oxide, whether before or after the sintering process. The apparent porosity is

an anti-phenotype behavior of Apparent density. This behavior corresponds to porous behavior (Yusoff and Hussain 2013, Efe *et al.* 2010).

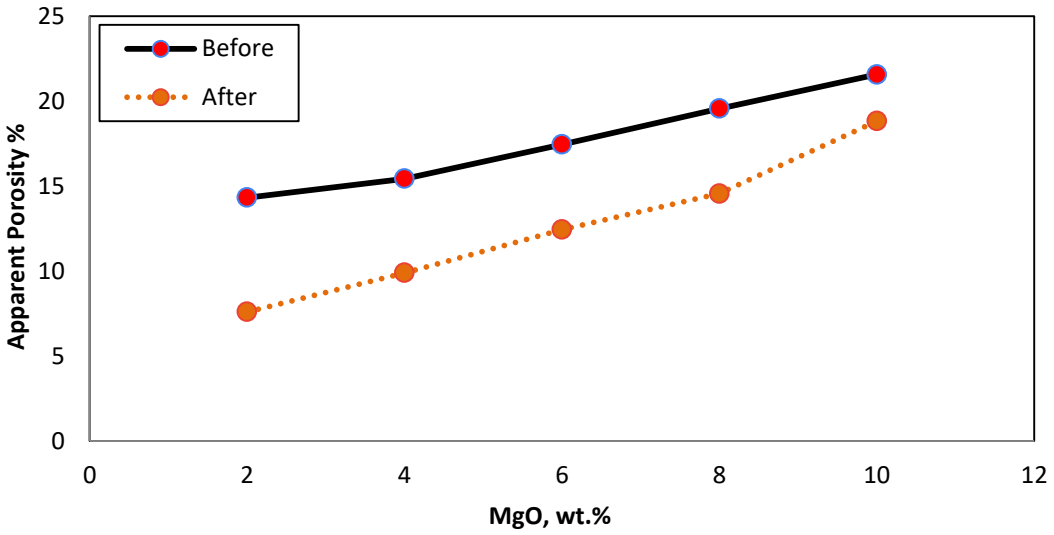


**Figure 5.3** Relation between reinforcement ratios of Cu-MgO nano and apparent porosity before and after sintering

### 5.1.4 Effect of nano MgO reinforcement content on apparent density

The relationship between the volumetric ratios of MgO nanoparticles and the apparent density before and after the sintering process indicates that the increase in the volumetric ratios of MgO nanoreinforcement led to a decrease in the apparent density earlier during the sintering process, as it decreased from 6.71-7.77 g/cm$^3$ in the MgO content material. nanoparticles 2-10%. In addition, the results proved that the increase in the volumetric ratios entered for the reinforcing material caused a decrease in the apparent density after sintering and a decrease in the surface density of 7.11-8.001 g/cm$^3$ when the MgO nano content material was from (2-10) percent due to the same reasons in paragraph Related to the actual density showing Figure 5.4.

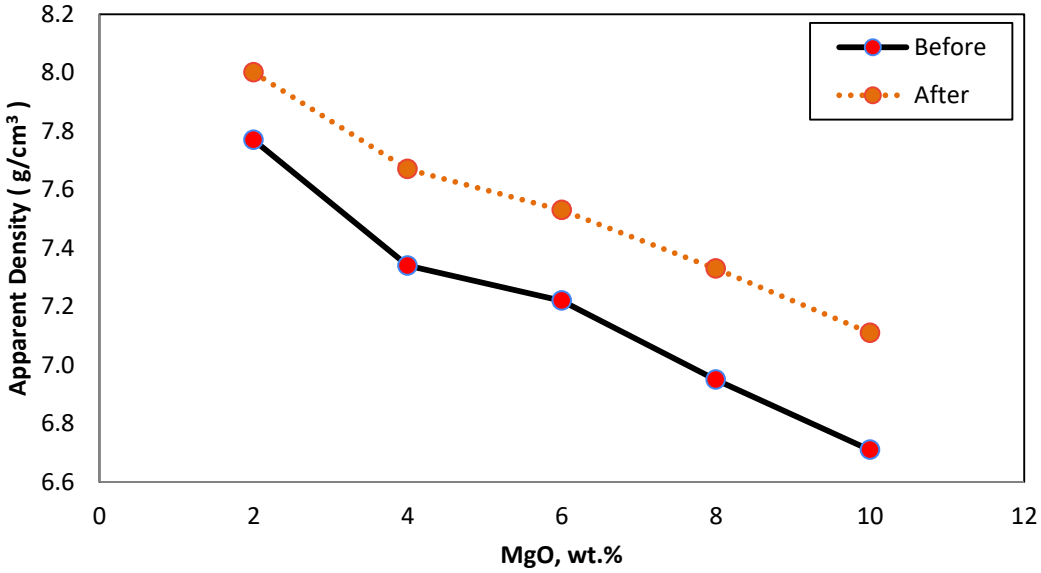


**Figure 5.4** Relation between reinforcement ratios of Cu-MgO nano and apparent density before and after sintering

### 5.1.5 Effect of nano MgO strengthening content on real porosity

We note from Figure 5.5 that the relationship between the change in the volumetric ratios of MgO nanoparticles and the real porosity before and after the sintering process, and the increase in the volumetric ratios added to the reinforcement material led to an increase in the real porosity before the sintering process from 14.34% at 2% of MgO nanoparticles to 27.01% at 10% of MgO nanoparticles. We also note that after the sintering process and increasing the volumetric proportions added to the reinforcement material. The true porosity increased after sintering from 9.98% nanoscale MgO to 20.25% at 10% nanoscale MgO.

The increase in real pores via increasing the content material of strengthening is that porosity is a reverse and result of density and since the density is reduced by growing the content of strengthening. It is essential to have a high pore ratio from the real porous ratio after the sintering compared to the real porosity ratio before the sintering. We note from Figure 5.5 that the percentage of real pores decreased after the sintering process. The reason for the decrease is the development of adhesion between the basis metal (Cu) and particle of the suppressed substance Nano MgO all through the sintering

method. The manner of sintering at a temperature of 900 °C for a couple of hours performs a first-rate position in shrinking the volume of pores in overlaps and decreasing porosity (Gan and Gu 2008, Efe *et al*. 2010, Noor Ahmed and Ramesh 2004).

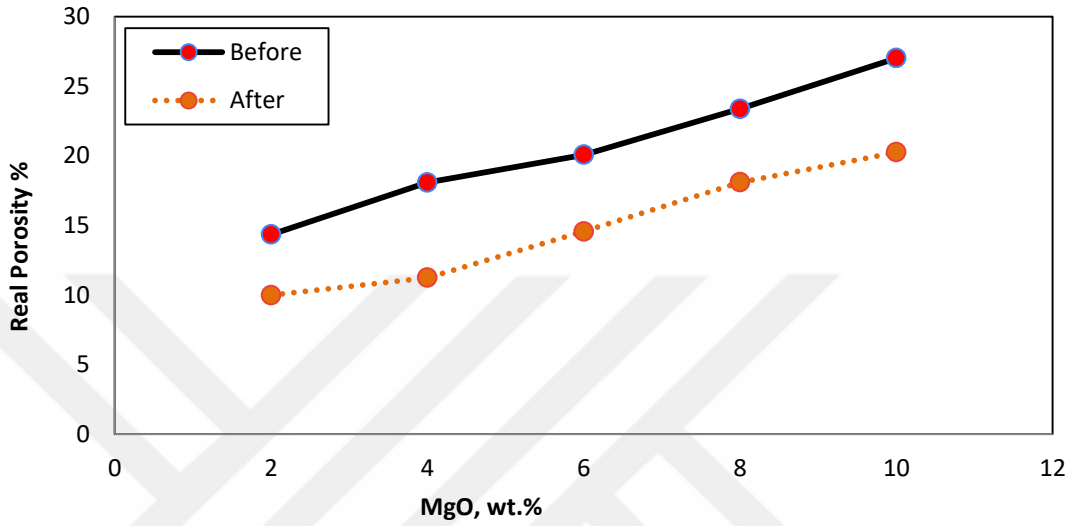


**Figure 5.5** Relation between reinforcement ratios of Cu-MgO nano and real porosity before and after sintering

### 5.1.6 Effect of nano MgO strengthening content on thermal conduction

We note from Figure 5.6 that thermal conductivity has decreased from 313 W/mK at 2% for nano MgO to 218 W/mK at 10% for nano magnesium oxide as the ratio increases. The volumetric of the strengthening material reduces thermal conductivity, and the decrease in thermal conductivity is due to the increase in the real porous ratio. It acts as an insulator within the overlapping particles, so any increase in its proportion necessarily reduces thermal conductivity and the weak thermal conductivity of oxide Nano-magnesium from 45-60 W/mK Compared to pure Cu 398 W/mK and Cu conductivity at room temperature 385 W/mK also exacerbate the negative effect of increasing the content of the booster material on thermal conductivity, the effect of the material in the packaging of contiguous Cu particles and the reduction of Cu pathways.

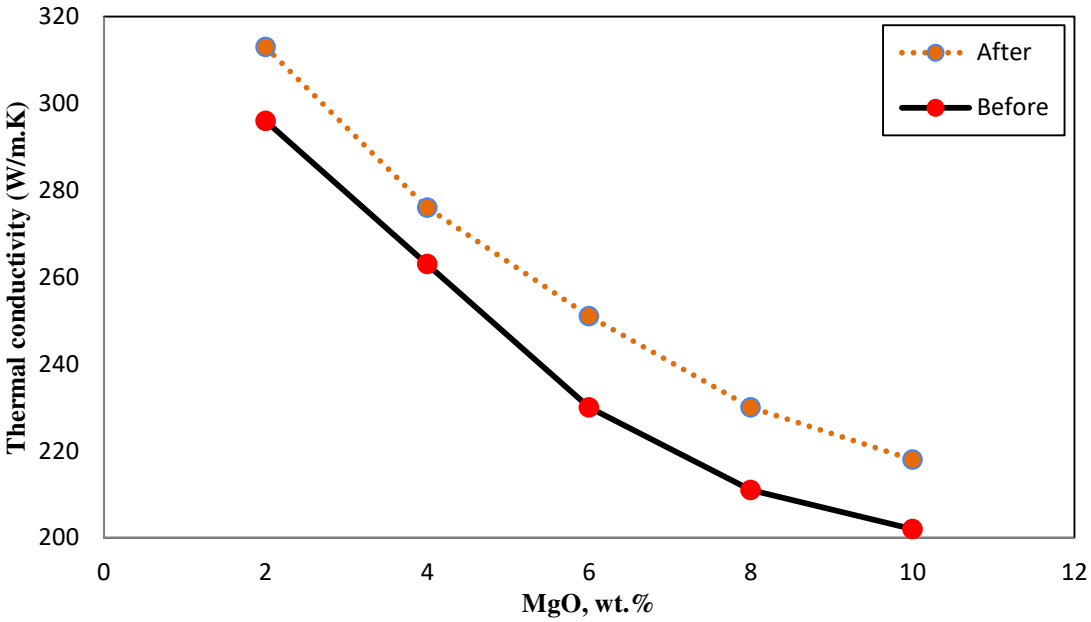


**Figure 5.6** Relation between reinforcement ratios of Cu-MgO nano and thermal conduction after sintering

## 5.2 Mechanical Properties

### 5.2.1 Impact of reinforcement content material on wear rate

The connection among the exchange in MgO Nanoparticles ratios and wear ratio before sintering at 900 °C for a couple of hours. It is noted that the heighten in volumetric ratios added caused a decrease in wear rate from ($3.43x10^{-4}$) g/cm at MgO nanoparticles content material (2)% to ($5.20x10^{-5}$) g/cm at MgO Nanoparticles content material (10)%. It is noted that the enhancement in MgO Nanoparticles volumetric ratios brought caused a lower in wear ratio from ($2.12x10^{-4}$) g/cm at MgO Nanoparticles content material (2)% to ($1.06x10^{-5}$) at MgO nanoparticles content material (10%). The low wear ratio of 6952 expand within the content material of reinforcement particles turned into because of that composites are tougher when adding MgO Nanoparticles, so weight loss is low because of reinforcement of the foundation or surface with MgO nanoparticles particle that impede the development of the dislocations as shown in Figure 5.7. Therefore, stresses resisted by challenging particles may be generated, after which a dislocated density might be generated. Right here, the difference in thermal

expansion coefficient will have a tremendous effect in this process, which leads to increased hardness through growing the content of reinforcement particles. Moreover, the wear ratio decreased with including particles (MgO Nanoparticles) that prompted heightened hardness. The applied wear ratio is inversely proportional to the hardness according to the following formula Equation (5.1) (Noor Ahmed and Ramesh 2004, Ghareeb *et al*. 2021):

$$V = K \times \frac{Wx}{H} \tag{5.1}$$

Where (V) is wear volume, (K) is (constant) wear coefficient, (W) is vertical load, (X) is sliding distance, and (H) is hardness of material.

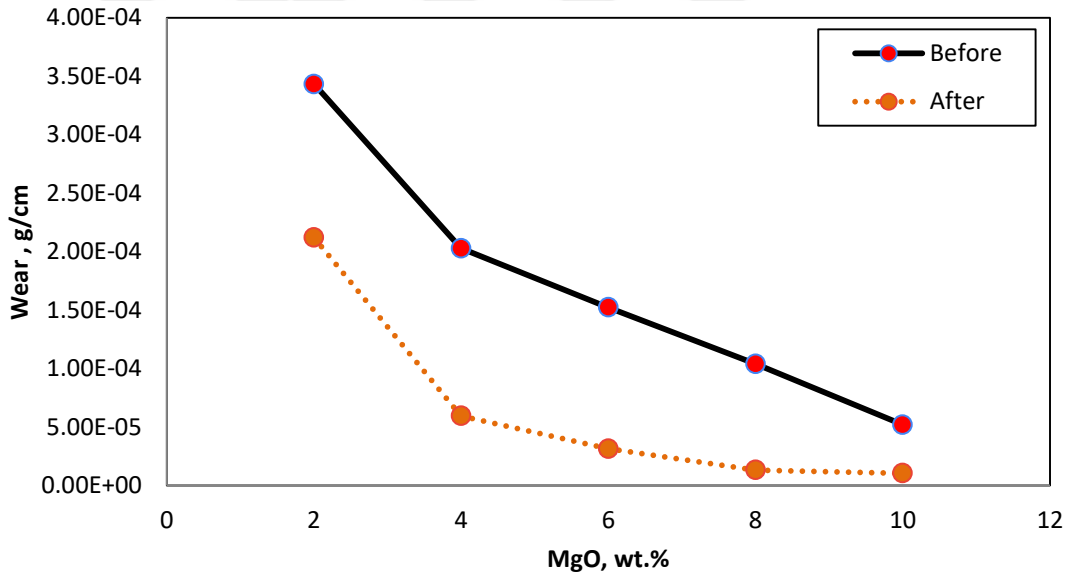


**Figure 5.7** Relation between reinforcement ratios of Cu-MgO nano and wear rate before and after sintering

### 5.2.2 Impact of reinforcement content on compressive strength

The relationship between the change in MgO Nanoparticles ratios and compressive stress before and after sintering shows that an increase in volumetric ratios led to elevated resistance to compressive stress. It extended (22-45) MPa while manganese content material from 2% to 10% resistance to compression after sintering also

expanded from (39-77) MPa at MgO Nanoparticles content (2-10)% before sintering (Figure 5.8). The heightened compressive stress with the heightened content material of reinforcement particles before and after sintering. In addition to growing the compressive stress strength values after sintering, there are higher than their previous values sintering because of the excessive resistance of reinforcement particles, which led to the expanded hardness of composites via growing MgO Nanoparticles. In addition to the especially powerful resistance to positional deformation and forming coherent specimens with excessive compressive power. The excessive sintering temperature for a couple of hours additionally performed a critical position in growing the bonding power among particles of components thru proper propagation and distribution, assisting and equipping the composite mass (Gan and Gu 2008).

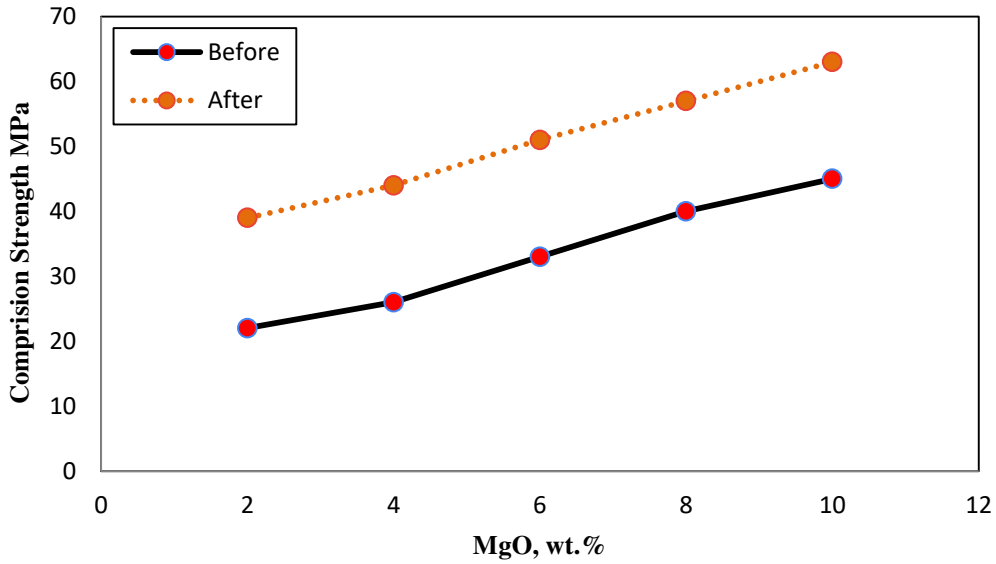


**Figure 5.8** Relation between reinforcement ratios of Cu-MgO nano and compressive strength before and after sintering

### 5.2.3 Impact of reinforcing content on hardness

The relation among the exchange in the volumetric ratios of MgO Nanoparticles on micro Vickers hardness before and after sintering shows an increase in volumetric ratios introduced led to improved hardness before sintering (39-88) Hv at MgO content from

(2%) to (10%). Hardness expanded after sintering (66-118) Hv at MgO content material of (2-10)% (Figure 5.9).

The increase in hardness before and after sintering is because of the addition of MgO Nanoparticles to the high hardness of MgO Nanoparticles, in addition to the variety of shapes because of the addition of reinforcement particles to MgO Nanoparticles. In addition to the increased resistance to elastic deformation and multiplied inner residual stresses. The different thermal expansion coefficients between the substrates and the reinforcement particle bring about many dislocations, which lead to accelerated hardness of composites due to the fact that MgO nanoparticles with high hardness act as obstacles to the deformation of the matrix. The boom in hardness after sintering is due to re-crystallization, granular increase, and elimination of stresses (ultimate after seven compaction tactics) in composites because of the high temperature of sintering to 900 °C for couple of hours (Al-Tounsi 1992).

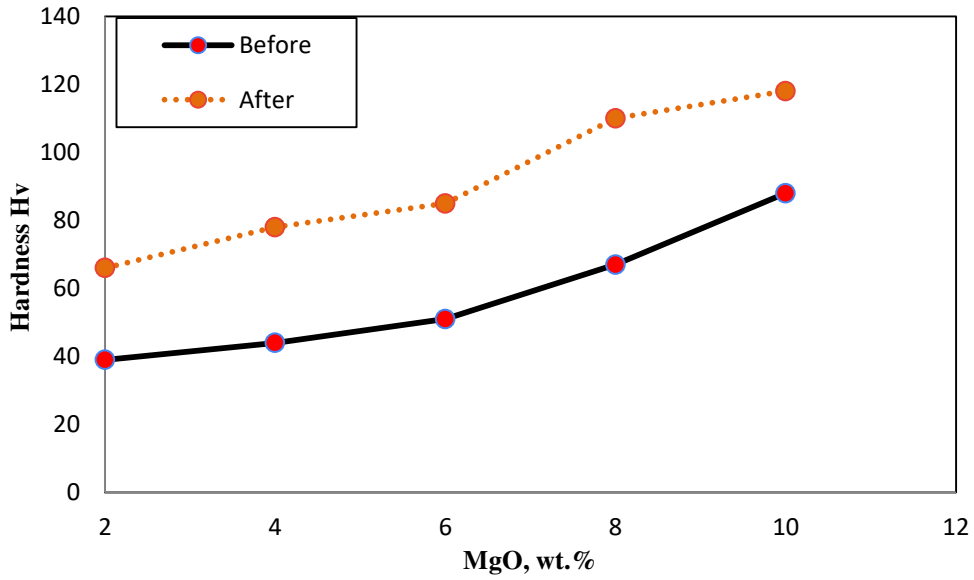


**Figure 5.9** Relation between reinforcement ratios of Cu-MgO nano and hardness before and after sintering

## 5.3 Synthetic Properties

### 5.3.1 Microstructure test

In this test, Figure 5.10, Figure 5.11, Figure 5.12, Figure 5.13 and Figure 5.14 represent the microstructure images of the overlaps after the process of sintering through the forms show that:

- The distribution of magnesium oxide homogeneously within the basis (copper) component of an interconnected metal mesh
- Recryslisation after sintering
- After sintering, the real porosity is less than it was beforehand.
- Magnesium Oxide nano particles are a center of porous polarization, whether before or after sintering.
- Lower granular-sized magnesium oxide nanoparticles attract more porous than larger granular-sized particles

**Figure 5.10** Magnified microscopic image 400 times for Specimen 1

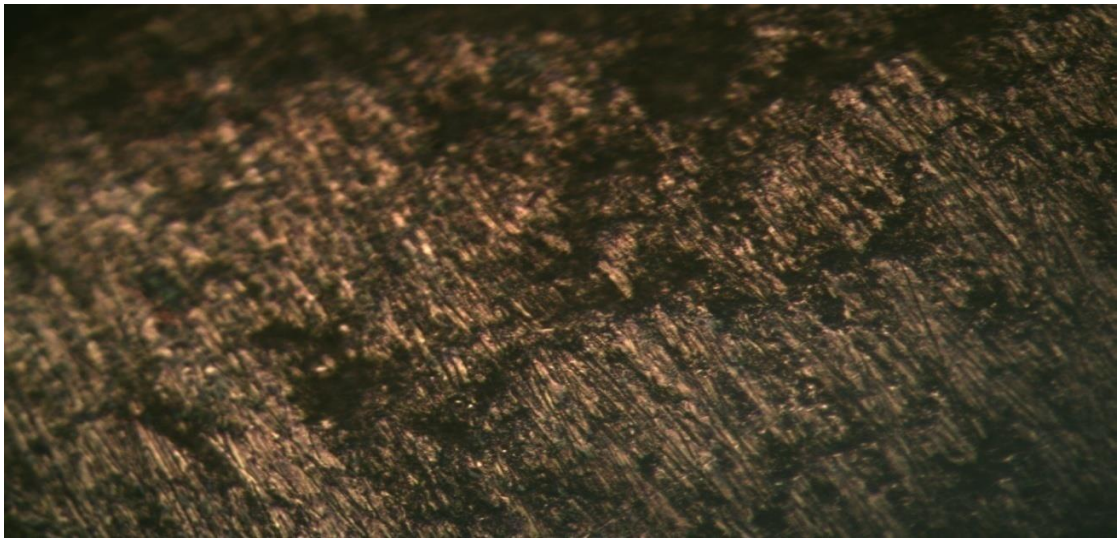

**Figure 5.11** Magnified microscopic image 400 times for Specimen 2

**Figure 5.12** Magnified microscopic image 400 times for Specimen 3

**Figure 5.13** Magnified microscopic image 400 times for Specimen 4

**Figure 5.14** Magnified microscopic image 400 times for Specimen 5

### 5.3.2 Impact of bolstering content on SEM test

Pics of a scanning electron microscope at (10μm) at different reinforcement ratios after the sintering specimens show a clear homogenization and distribution of MgO nanoparticles. This is the reason for the increase in the ratio of hardness and porosity after the process of solidification and less porosity before the process of sintering and as a result of the process of sintering and the appropriate heat that has a good effect on the convergence of the particles and overlapping materials (Figure 5.15) (a, b, c, d, e).

### 5.3.3 Impact of bolstering content on EDS or EDX test

The consequence of the X-ray spectrometer EDS showed an enormous correlation between forces and homogeneity between the particles of the components and interference between the particles of the materials, and the convergence of the molecules from each other. We note that there are not any cracks or divisions. This indicates that the heat treatment has a good effect on the interconnectedness and convergence of the materials, and the disappearance is clear to the attributes and defects. As shown in picture C, the MgO nanoparticles were the centers of porosity polarisation. For specimen 5, we notice the beginning of dislocation and the appearance of porosity, demonstrating that the fine support ratios are 10% (Figure 5.16).

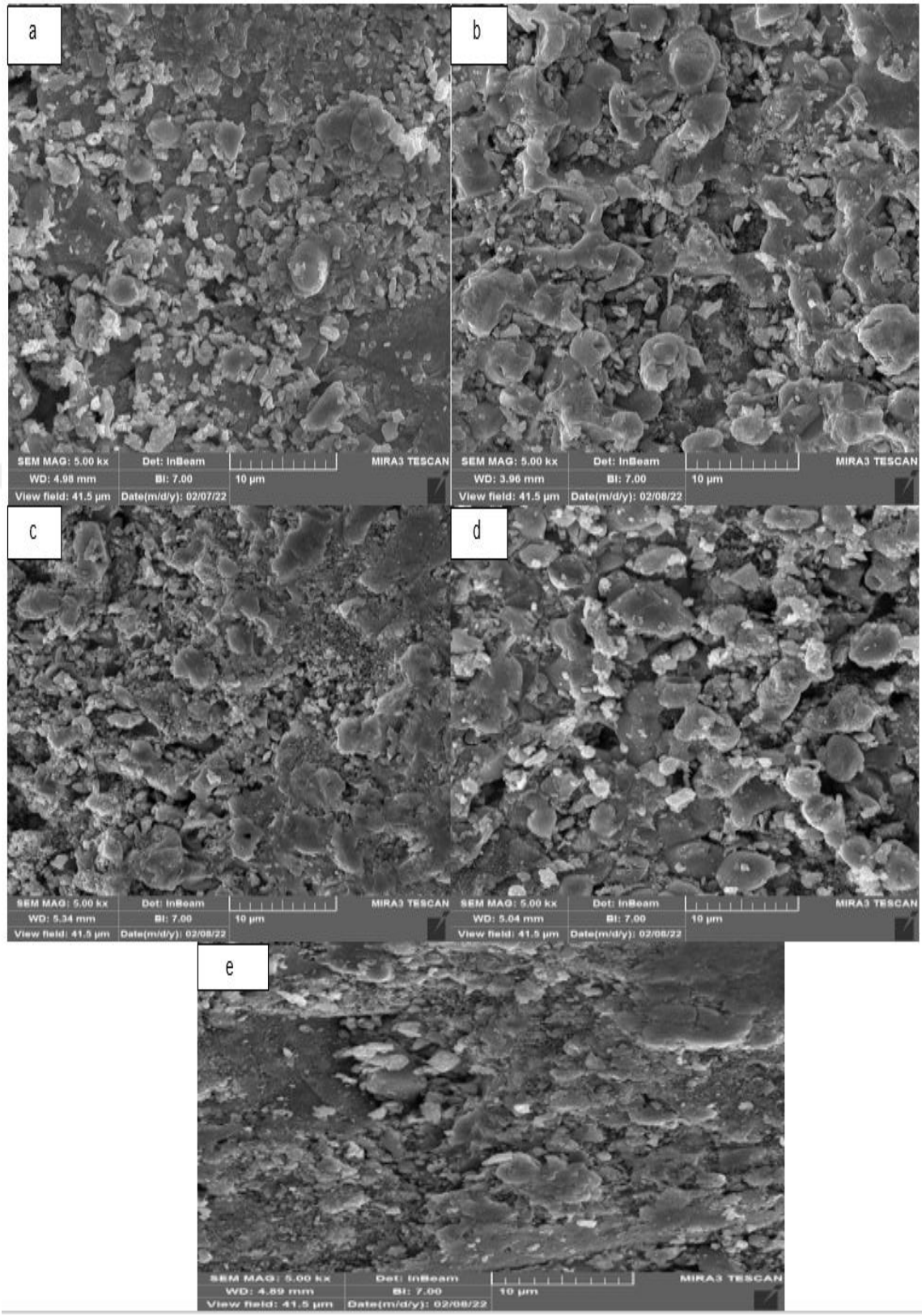


**Figure 5.15** The following are images taken with a scanning electron microscope of the overlaid (Cu-MgO) after sintering with extraordinary reinforcement ratios. (a-2%, b-4%, c-6%, d-8%, e-10%)

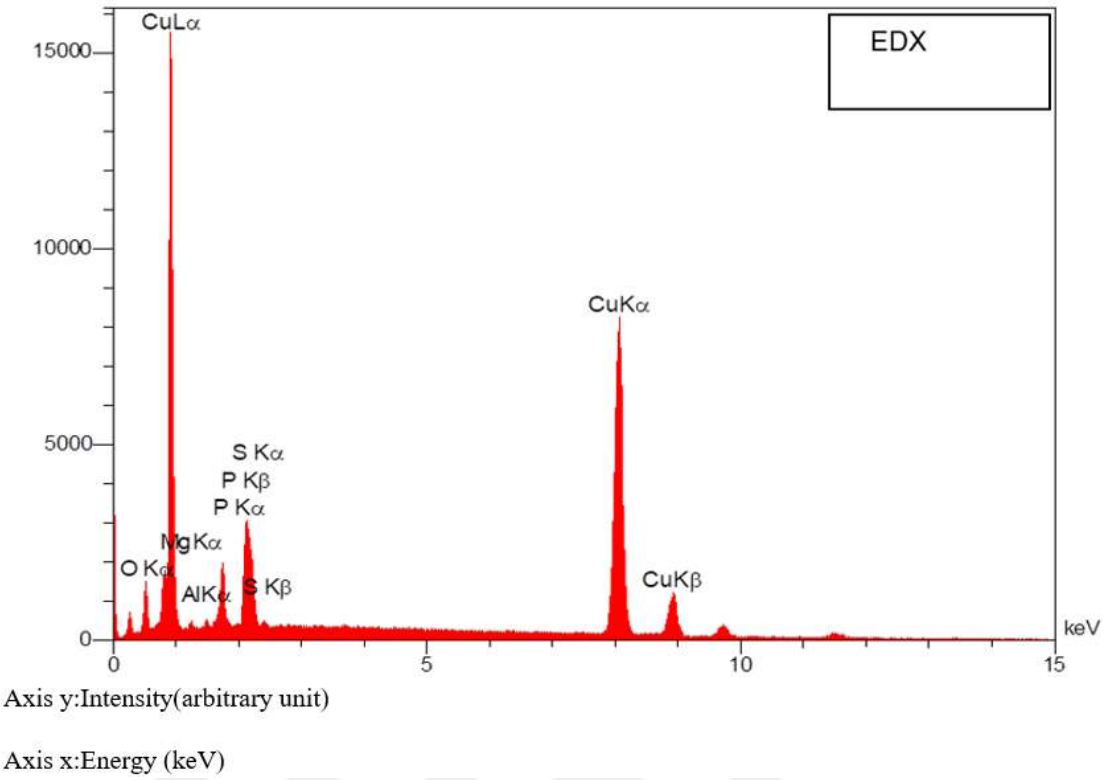


**Figure 5.16** EDX test results

### 5.3.4 X-ray diffraction results

The study of specimens through X-rays is an important means of identifying the nature and composition of overlapping materials and monitoring the changes of the crystalline (Cu) when conducting the process of piston and sintering at 900 ℃. For a couple of hours in this form, an XRD x-ray was examined at different support ratios of Nano-Magnesium Oxide (2, 4, 6, 8, 10)% after sintering. We note the appearance of the base material at the international card number (Figure 5.17) (Figure 5.18) (Figure 5.19) (Figure 5.20) (Figure 5.21).

Cubic, Cu Card No.01-085-1326) and crystalline cube phase at Miller coefficients (111), (200), (220), and this is fully compatible with the global measurement. We also note the appearance of the aggregate oxide Nano at cubic, MgO Nanoparticles (Card No.00-0043-1022) and crystal cube phase at Miller transactions (111), (200), (220), (311) as shown in Table 5.1.

This is also fully compatible with the global measurement, where we note a rise in the peaks of both the base material Cu and the material.

Strengthening the nano-magnesium magnesium with an increase in the percentage of reinforcement indicates the spread of the strengthening material during the base material, and the atoms are more regular. This is confirmed in the mechanical and physical test results that we observed have improved with the increase in volumetric strengthening (Figure 5.22) (Figure 5.23) (Figure 5.24).

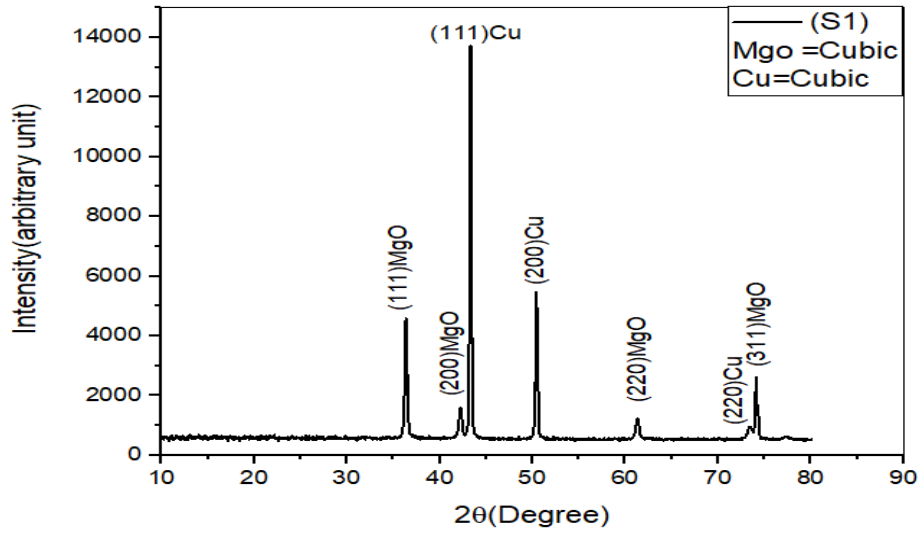


**Figure 5.17** X-ray diffraction for specimen 1 and Miller coefficients

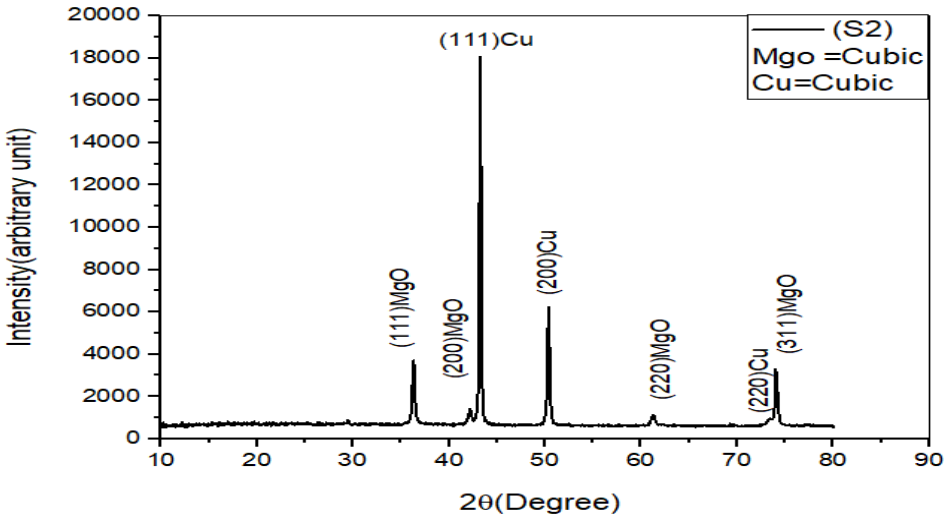


**Figure 5.18** X-ray diffraction for specimen 2 and Miller coefficients

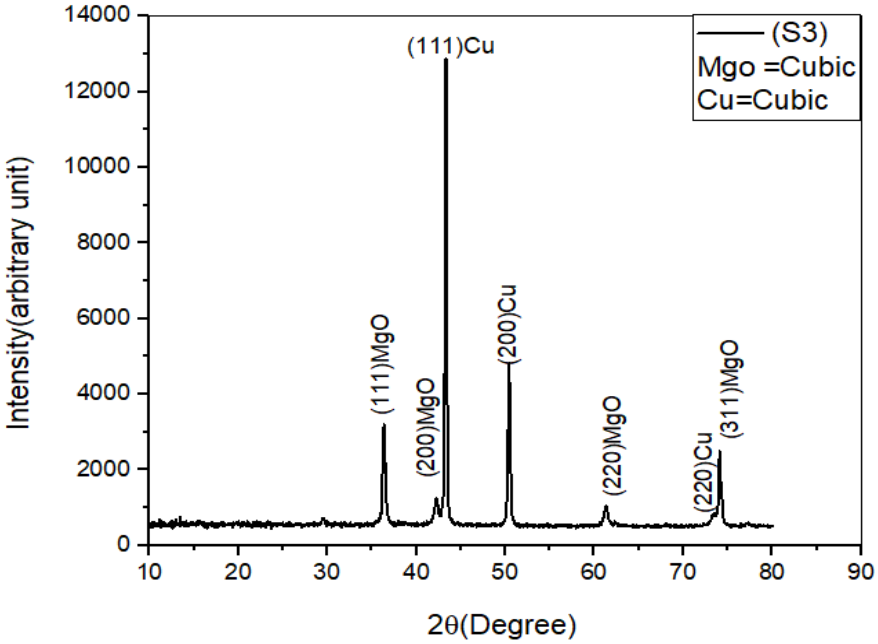


**Figure 5.19** X-ray diffraction for specimen 3 and Miller coefficients

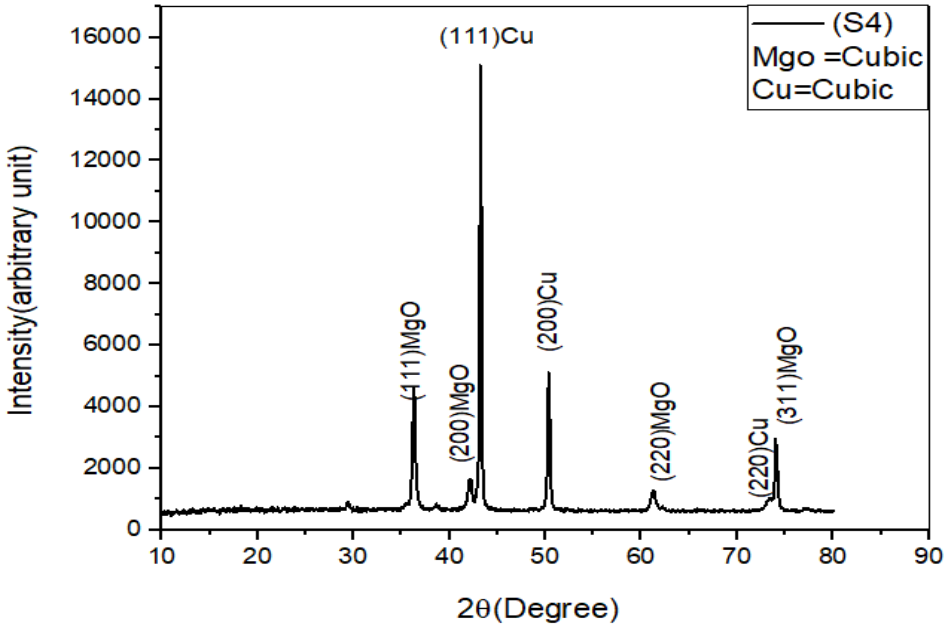


**Figure 5.20** X-ray diffraction for specimen 4 and Miller coefficients

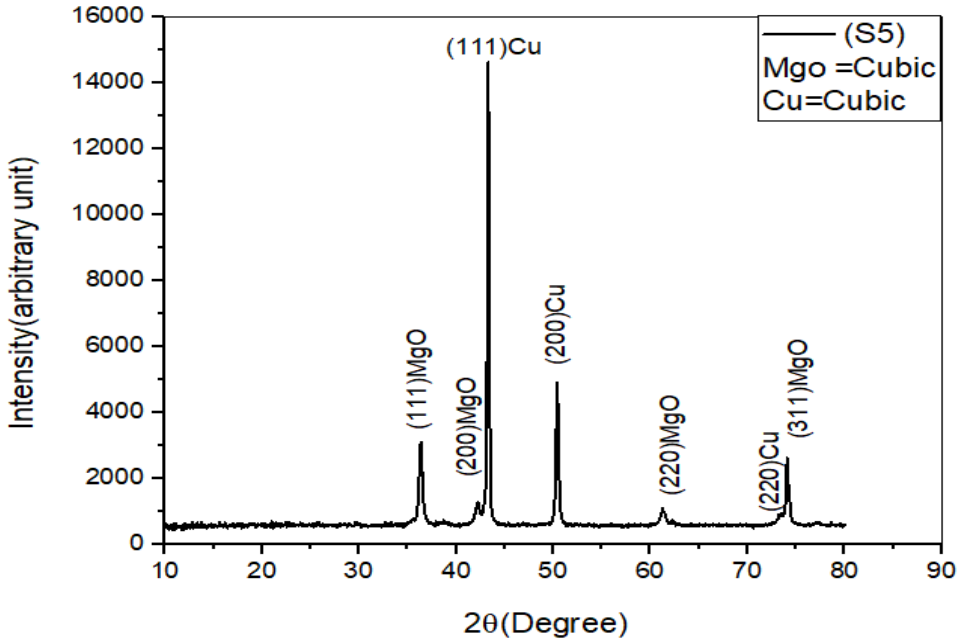


**Figure 5.21** X-ray diffraction for specimen 5 and Miller coefficients

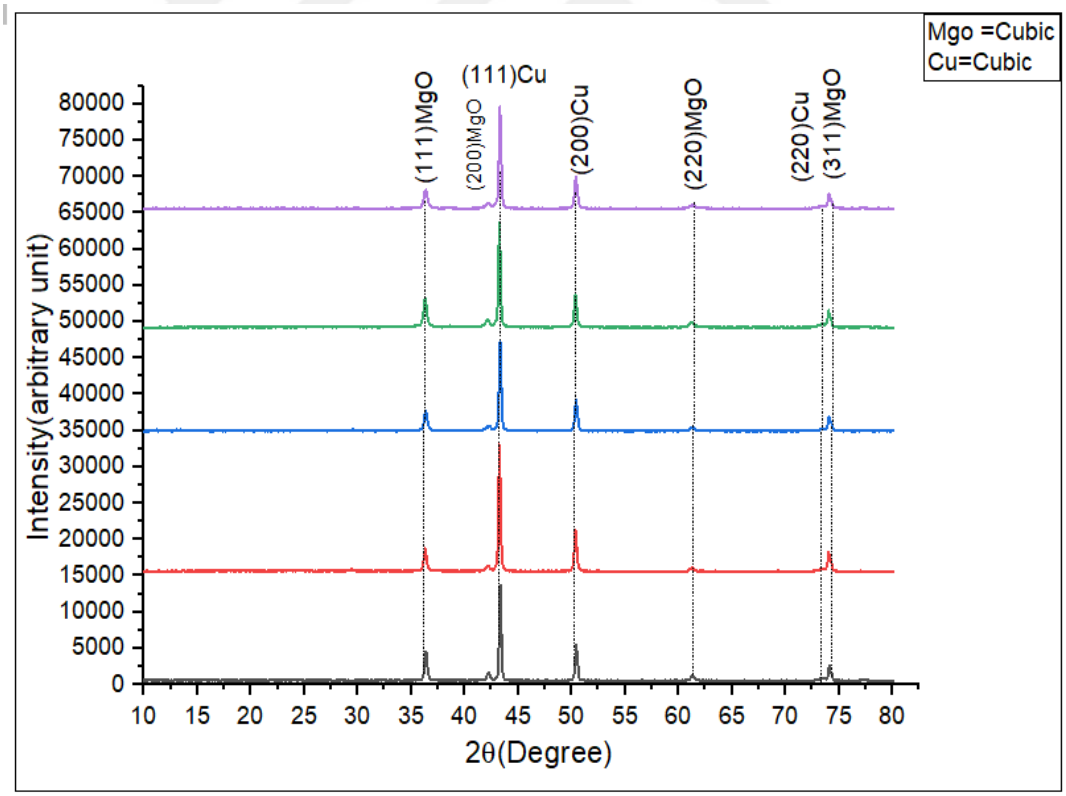


**Figure 5.22** X-ray diffraction of specimenes and Miller coefficients at different reinforcement ratios after plastering and sintering

**Table 5.1** Phase, Standard Number, Card Number and Angle for Cu-MgO

| Energy (mJ) | 2θ (Deg.) | FWHM (Deg.) | $d_{hkl}$ Exp.(Å) | G.S (nm) | Phase | hkl | Card No. |
|---|---|---|---|---|---|---|---|
| | 36.36512 | 0.30529 | 2.46854831 | 4.506708178 | (Cubic)MgO | -111 | 00-043-1022 |
| | 42.2276 | 0.41585 | 2.138406481 | 3.248633203 | (Cubic)MgO | -200 | 00-043-1022 |
| $S_1$ | 43.3214 | 0.22323 | 2.086915351 | 6.029222328 | (Cubic)Cu | -111 | 01-085-1326 |
| | 50.4405 | 0.2655 | 1.807795598 | 4.934538448 | (Cubic)Cu | -200 | 01-085-1326 |
| | 61.30339 | 0.42053 | 1.510931912 | 2.962523469 | (Cubic)MgO | -220 | 00-043-1022 |
| | 73.42914 | 0.50576 | 1.288495508 | 2.29532289 | (Cubic)Cu | -220 | 01-085-1326 |
| | 74.14049 | 0.34229 | 1.277883289 | 3.375751054 | (Cubic)MgO | -311 | 00-043-1022 |
| | 36.30222 | 0.34333 | 2.47268108 | 4.507519995 | (Cubic)MgO | -111 | 00-043-1022 |
| | 42.89438 | 1.83291 | 2.106696838 | 3.241278958 | (Cubic)MgO | -200 | 00-043-1022 |
| $S_2$ | 43.25546 | 0.22277 | 2.089943809 | 6.030599226 | (Cubic)Cu | -111 | 01-085-1326 |
| | 50.36539 | 0.2948 | 1.8103153 | 4.93606077 | (Cubic)Cu | -200 | 01-085-1326 |
| | 61.26255 | 0.44617 | 1.51184122 | 2.963148985 | (Cubic)MgO | -220 | 00-043-1022 |
| | 73.39698 | 0.51669 | 1.288980627 | 2.295803212 | (Cubic)Cu | -220 | 01-085-1326 |
| | 74.07967 | 0.37267 | 1.278781867 | 3.377104165 | (Cubic)MgO | -311 | 00-043-1022 |
| | 36.35872 | 0.37832 | 2.468968149 | 4.506790841 | (Cubic)MgO | -111 | 00-043-1022 |
| | 42.82113 | 1.83753 | 2.110130807 | 3.242092239 | (Cubic)MgO | -200 | 00-043-1022 |
| $S_3$ | 43.31139 | 0.22584 | 2.087374476 | 6.029431476 | (Cubic)Cu | -111 | 01-085-1326 |
| | 50.4188 | 0.30603 | 1.808522763 | 4.934978479 | (Cubic)Cu | -200 | 01-085-1326 |

**Table 5.1** Phase, Standard Number, Card Number and Angle for Cu-MgO (Continued)

| Energy (mJ) | 2θ (Deg.) | FWHM (Deg.) | $d_{hkl}$ Exp.(Å) | G.S (nm) | Phase | hkl | Card No. |
|---|---|---|---|---|---|---|---|
| | 61.30541 | 0.5291 | 1.510886969 | 2.962492521 | (Cubic)MgO | -220 | 00-043-1022 |
| | 73.42721 | 0.61824 | 1.288524608 | 2.295351721 | (Cubic)Cu | -220 | 01-085-1326 |
| | 74.12357 | 0.38135 | 1.278133109 | 3.376127582 | (Cubic)MgO | -311 | 00-043-1022 |
| | 36.29625 | 0.38364 | 2.47307409 | 4.507596976 | (Cubic)MgO | -111 | 00-043-1022 |
| | 42.64749 | 1.84098 | 2.118319437 | 3.244014837 | (Cubic)MgO | -200 | 00-043-1022 |
| | 43.25104 | 0.22424 | 2.090147148 | 6.030691449 | (Cubic)Cu | -111 | 01-085-1326 |
| $S_4$ | 50.3566 | 0.30138 | 1.810610686 | 4.936238787 | (Cubic)Cu | -200 | 01-085-1326 |
| | 61.23646 | 0.58398 | 1.512422791 | 2.963548389 | (Cubic)MgO | -220 | 00-043-1022 |
| | 73.59837 | 1.31379 | 1.285950418 | 2.2927924 | (Cubic)Cu | -220 | 01-085-1326 |
| | 74.07452 | 0.33036 | 1.278858029 | 3.377218697 | (Cubic)MgO | -311 | 00-043-1022 |
| | 36.35233 | 0.44037 | 2.469387482 | 4.506873361 | (Cubic)MgO | -111 | 00-043-1022 |
| | 42.86182 | 1.77141 | 2.108221768 | 3.241640629 | (Cubic)MgO | -200 | 00-043-1022 |
| | 43.30222 | 0.22761 | 2.087795264 | 6.029623033 | (Cubic)Cu | -111 | 01-085-1326 |
| $S_5$ | 50.40739 | 0.3262 | 1.808905372 | 4.93520978 | (Cubic)Cu | -200 | 01-085-1326 |
| | 61.29299 | 0.65506 | 1.511163347 | 2.962682794 | (Cubic)MgO | -220 | 00-043-1022 |
| | 73.37549 | 0.70595 | 1.289305055 | 2.296124072 | (Cubic)Cu | -220 | 01-085-1326 |
| | 74.11878 | 0.39863 | 1.278203855 | 3.376234163 | (Cubic)MgO | -311 | 00-043-1022 |

**Name and formula**

Reference code: 00-043-1022

Mineral name: Periclase, syn
PDF index name: Magnesium Oxide

Empirical formula: MgO
Chemical formula: MgO

**Crystallographic parameters**

Crystal system: Cubic
Space group: Fm-3m
Space group number: 225

a (?): 4.2130
b (?): 4.2130
c (?): 4.2130
Alpha (°): 90.0000
Beta (°): 90.0000
Gamma (°): 90.0000

Calculated density (g/cm^3): 3.59
Volume of cell (10^6 pm^3): 74.78
Z: 4.00

RIR: 3.03

**Status, subfiles and quality**

Status: Marked as deleted by ICDD
Subfiles: Inorganic
Mineral
Alloy, metal or intermetalic
Corrosion
Pharmaceutical
Quality: Calculated (C)

**Comments**

Deleted by: Deleted by 45-946, experimental pattern; minerals subcommittee 6/94 .

General comments: Calculation of diffractometer peak intensities done with M POWD v. 2.2 (D. Smith and K. Smith) using default instru broadening function (NBS Table), diffracted beam monochromator polarization correction, and atomic scatt factors corrected for anomalous dispersion. Cell parame from Sasaki, S. et al ‹.*Proc. Jpn. Acad* .(1979) 48-43 **55** ‹ Atomic positions from same source: Mg in 2a, O in 1b. Isotropic thermal parameters also from same source: Mg B=.31 ‹2O, B=.362 .

**References**

Primary reference: Grier, D., McCarthy, G., North Dakota State University, Fargo, North Dakota, USA ‹.*ICDD Grant-in-Aid*(1991) ‹

**Peak list**

| No. | h | k | l | d [A] | 2Theta[deg] | I [%] |
|---|---|---|---|---|---|---|
| 1 | 1 | 1 | 1 | 2.43200 | 36.931 | 11.0 |
| 2 | 2 | 0 | 0 | 2.10600 | 42.909 | 100.0 |
| 3 | 2 | 2 | 0 | 1.48950 | 62.283 | 51.0 |
| 4 | 3 | 1 | 1 | 1.27030 | 74.658 | 6.0 |
| 5 | 2 | 2 | 2 | 1.21620 | 78.598 | 15.0 |
| 6 | 4 | 0 | 0 | 1.05320 | 94.006 | 6.0 |
| 7 | 3 | 3 | 1 | 0.96650 | 105.689 | 3.0 |
| 8 | 4 | 2 | 0 | 0.94210 | 109.699 | 18.0 |

**Stick Pattern**

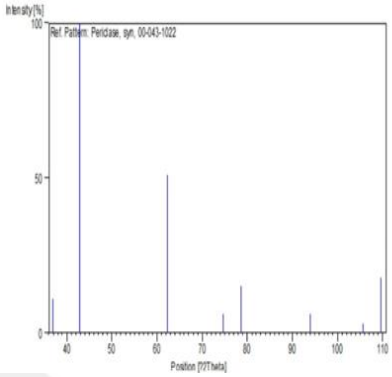


**Figure 5.23** MgO Nano Card

**Name and formula**

Reference code: 01-085-1326

Mineral name: Copper
ICSD name: Copper

Empirical formula: Cu
Chemical formula: Cu

**Crystallographic parameters**

Crystal system: Cubic
Space group: Fm-3m
Space group number: 225

a (?): 3.6150
b (?): 3.6150
c (?): 3.6150
Alpha (°): 90.0000
Beta (°): 90.0000
Gamma (°): 90.0000

Calculated density (g/cm^3): 8.93
Measured density (g/cm^3): 8.96
Volume of cell (10^6 pm^3): 47.24
Z: 4.00

RIR: 8.86

**Subfiles and Quality**

Subfiles: Inorganic
Mineral
Alloy, metal or intermetalic
Corrosion
Modelled additional pattern
Quality: Calculated (C)

**Comments**

Additional pattern: See PDF 4-836 .
ICSD collection code: 064699
Test from ICSD: No R value given.
At least one TF missing .

**References**

Primary reference: *Calculated from ICSD using POWD-12*(1997) ‹++
Structure: Swanson, H.E., Tatge, E ‹.*Natl. Bur. Stand. (U.S.), Circ.* (1953) ‹1 ‹**359**

**Peak list**

| No. | h | k | l | d [A] | 2Theta[deg] | I [%] |
|---|---|---|---|---|---|---|
| 1 | 1 | 1 | 1 | 2.08712 | 43.317 | 100.0 |
| 2 | 2 | 0 | 0 | 1.80750 | 50.449 | 42.7 |
| 3 | 2 | 2 | 0 | 1.27810 | 74.126 | 17.1 |
| 4 | 3 | 1 | 1 | 1.08996 | 89.938 | 15.6 |

**Stick Pattern**

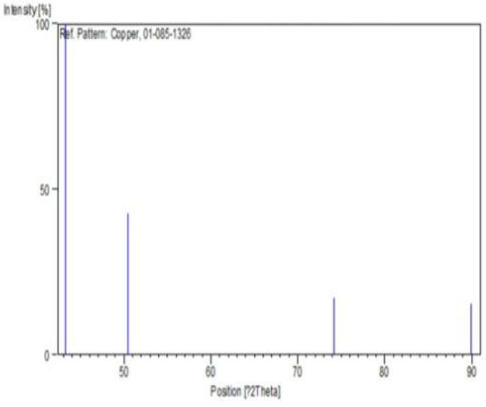


**Figure 5.24** Cu Card

## 6. CONCLUSIONS AND RECOMMENDATION

The important result of this study is the possibility of promoting nano MgO with a different metal material, obtaining specimens with good physical, mechanical and synthetic properties, and the possibility of pressing powders Cu-Nano MgO with powder technology and homogenizing the distribution of nano MgO. In copper base, significantly for all specimens prepared through microstructure test and decrease or decrease of both volumetric density, Apparent density, and green density. For overlaps by increasing the content of Nano MgO.

Real porosity and Apparent porosity increase water absorption of overlays by increasing the content of nano MgO before and after the sintering system; however, after the sintering, it is far decreased than the pre-sintering ratios. This is due to improved adhesion between Cu-Nano MgO during the sintering process due to the 900 °C s sintering process for a couple of hours that played a role in shrinking the scale of pores and decreasing porosity in overlays and that the hardness increased before and after the sintering process by increasing the strengthening content. Concerning the erosion rate, the increased strengthening content and thermal conductivity have decreased as the volumetric ratio of Nano MgO increases due to an increase in the proportion of real porosity that acts as insulators within the overlays.

As for the compression force before and after the sintering process, which increased the volumetric ratios of the strengthening material according to the results (SEM) and the results of the test (EDX), there was evidence that the awareness of the weapon extended with every pattern. As for the fifth specimen, which had a strengthening content material ratio of 10% of Nano MgO, we find the start of dislocation and the appearance of pores, which indicates that it is by far the excellent help ratio.

Through the XRD test, we observed a rise in the tops of both the base material and the strengthening material, with an increase in the volumetric ratios of the strengthening material, indicating the spread of the strengthening material through the base material.

## 6.1 Recommendations

- It is recommended to study of the electrical properties of the overlay (Cu-MgO).
- It is recommended to the effect of describing other components to the overlapping (Cu-MgO).
- It is recommended to study the process of sintering with plasma flame or microwaves or emptying the properties of the overlapping (Cu- MgO).
- It is recommended to study of the volumetric and granular effect and volumetric distribution of copper powder to overlap on physical, synthetic and mechanical properties.

## REFERENCES


Abdel-Wahab, A. A., Ataya, S. and Silberschmidt, V. V. 2017. Temperature-dependent Mechanical behaviour of PMMA: Experimental analysis and modelling. Polymer Testing, 58: 86-95.

Al-Sharifi, S. M. H. 2007. Impact of plumbing elements and thermal treatment on the behaviour of the base alloy Cu–Al. MSc. Thesis, University of Babylon, 98 page, Babylon.

Al-Tounsi, A. 1992. Effect of sintering parameters on the mechanical and physical properties of sinter formed materials. PhD. Thesis, Dublin City University, 178 page, Dublin.

Amori, A. A. 2008. The effect of adding Nickel element to alloy (Al-4%, Cu-1.5% Mg). MSc. Thesis, University of Technology, 117 page, Sydney.

Balamurugan, E., Sethuraman, N., Sudagar, S. and Arun, A. 2015. Wear behaviour of hybrid (AL+ SiC+ Al2O3) Metal Matrix Composite. International Journal of Emerging Technology and Advanced Engineering, 5(12): 2250-2459.

Bruls, R. J. 2002. The thermal conductivity of magnesium silicon nitride ceramics and related materials. Universiteitsdrukkerij Technische Universiteit Eindhoven, 2(2).

Cardarelli, F. 2008. Materials handbook: a concise desktop reference. International Journal of Materials Research, 10: 31-39.

Chawla, N., and Chawla, K. K. 2006. Interface. Metal Matrix Composites, 113-136.

Clyne, T. W. and Withers, P. J. 1995. An introduction to metal matrix composites. Cambridge University Press, 509 page, Cambridge.

Cullity, B. D. 1956. Elements of X-ray Diffraction. Addison-Wesley Publishing, 529 page, New York.

Efe, G. C., Altinsoy, I., Yener, T., Ipek, M., Zeytin, S. and Bindal, C. 2010. Characterization of cemented Cu matrix composites reinforced with SiC. Vacuum, 85(5): 643-647.

Emara, M. M. 2014. The Effect of Particle Alignment on the Tensile Behaviors of Extruded Al2O3/2124 Aluminum Alloy Metal Matrix Composites. Journal of Materials Science and Engineering, 4(1A).

Gan, K. and Gu, M. 2008. The compressibility of Cu/SiCp powder prepared by high-energy ball milling. Journal of Materials Processing Technology, 199(1-3): 173-177.

Ghareeb, S. M., Allah, S. M. A. and Darweesh, S. Y. 2021. Compressive strength, wear, and structure characteristics as a result of silicon carbide addition on a copper base. Journal of Physics: Conference Series. IOP Publishing, 1999(1): 12-40.

Giri, S., Sahu, D. K., Sarkar, N. N. and Rewatkar, K. G. 2021. Study of structural and magnetic properties of aluminium-substituted nanosized barium hexaferrite prepared by sol–gel auto-combustion Technique. Bulletin of Materials Science, 44(2): 1-8.

Gohar, G. A., Manzoor, T., Ahmad, A., Raza, H., Farooq, A., Karim, I. and Asad, F. 2020. Synthesis and investigate the properties of Cu–Al–Ni alloys with Ag addition using powder metallurgy Technique. Journal of Alloys and Compounds, 817: 153281.

Griffin, R. B. 2006. An experiment in powder metallurgy–sintering of Cu. Department of Mechanical Engineering, Texas A. and M. University, College Station, TX 77843: 1-14.

Groover, M. P. 2020. Fundamentals of modern manufacturing: materials, processes, and systems. John Wiley & Sons, 816 page, New York.

Haynes, W. M., Lide, D. R. and Bruno, T. J. 2016. CRC handbook of chemistry and physics. CRC press, 2664 page, Boca Raton.

Heba, J. J. 2010. Fiber's impact on the behavior of the suppression of polymer-based overlapping materials. MSc. Thesis, University of Technology, 69 page, Sydney.

Hedjazi, G. 2009. Assessment of processing techniques for Orthopaedic Composites. Digitala Vetenskapliga Arkivet, 9(4): 1-11.

Jabur, A. S. 2013. Effect of powder metallurgy conditions on the properties of porous bronze. Powder Technology, 237: 477-483.

Jin, Y. and Hu, M. 2011. Densification of graphite/copper compound powders. In 2011 Second International Conference on Mechanic Automation and Control Engineering. IEEE, 1131-1135.

Kandiban, M., Vigneshwaran, P. and Potheher, I. V. 2015. Synthesis and characterization of mgo nanoparticles for photocatalytic applications. In

Department of Physics, Bharathidasan Institute of Technology (BIT) Campus, Anna University, Tiruchirappalli, Tamilnadu, India, Conference Paper, 2015.

Karim, A. S., Majeed, Z. N. and Darweesh, S. Y. 2021. The Effect of nanostructured Zirconia reinforcement on the mechanical and structural properties of a copper-based system. In Materials Science Forum. Trans Tech Publications, 1039: 297-306.

Lee, P. W., Trudel, Y., Iacocca, R., German, R. M., Ferguson, B. L., Eisen, W. B. and Moyer, K. 1998. Warm Compaction. Powder Metal Technologies and Applications, 7: 376-381.

Lipowsky, H. and Arpaci, E. 2008. Copper in the automotive industry. John Wiley & Sons, 191 page, New York.

Mei, A. B., Hellman, O., Schlepütz, C. M., Rockett, A., Chiang, T. C., Hultman, L. and Greene, J. E. 2015. Reflection thermal diffuse x-ray scattering for quantitative determination of phonon dispersion relations. Physical Review B, 92(17): 174301.

Miracle, D. B. and Donaldson, S. L. 2001. Introduction to composites. ASM Handbook, 21: 3-17.

Moustafa, S. F., El-Badry, S. A., Sanad, A. M. and Kieback, B. 2002. Friction and wear of copper–graphite composites made with Cu-coated and uncoated graphite powders. Wear, 253(7-8): 699-710.

Nazarian-Samani, M., Kamali, A. R., Mobarra, R. and Nazarian-Samani, M. 2010. Phase transformations of Ni-15 wt.% B powders during Mechanical alloying and annealing. Materials Letters, 64(3): 309-312.

Noor Ahmed, R. and Ramesh, C. S. 2004. Tribological properties of cast Copper–SiC–Graphite Hybrid composites. nternational Symposium on Applied Engineering and Sciences, 2004: 22-24

Ramakrishnan, P. 1983. Department of metallurgical engineering, Indian Institute of Technology, Bombay 400 076 (Received 19 January 1980). Indian Journal of History of Science, 18(1): 109-114.

Ropp, R. C. 2012. Encyclopedia of the alkaline earth compounds. Newnes, 1216 page, Londra.

Saha, J., Begum, A., Mukherjee, A. and Kumar, S. 2017. A novel green synthesis of silver nanoparticles and their catalytic action in reduction of Methylene Blue dye. Sustainable Environment Research, 27(5): 245-250.

Salih, E. J., Allah, S. M. A., Darweesh, S. Y. and Mohammed, H. A. 2021. Study of some of the physical variables of a metal-based system using the powder method. In Journal of Physics: Conference Series. IOP Publishing, 99(1): 12-18.

Singh, D. P., Yadav, R. M. and Yadav, T. P. 2012. Synthesis of Metal Vanadate Nanostructures. Reviews in Advanced Sciences and Engineering, 1(4): 319-341.

Smith, K. C. A. and Oatley, C. W. 1955. The scanning electron Microscope and its fields of application. British Journal of Applied Physics, 6(11): 391.

Taurian, O. E., Springborg, M. and Christensen, N. E. 1985. Self-consistent electronic structures of MgO and SrO. Solid State Communications, 55(4): 351-355.

Upadhyaya, G. S. 1997. Powder metallurgy Technology. Cambridge International Science Publishing, 158 page, Cambridge.

Venkatesh, B. and Harish, B. 2015. Mechanical properties of metal matrix composites (Al/SiCp) particles produced by powder metallurgy. International Journal of Engineering Research and General Science, 3(1): 1277-1284.

Vigneshwaran, N., Prasad, V., Arputharaj, A., Bharimalla, A. K. and Patil, P. G. 2018. Nano-zinc oxide: prospects in the textile industry. Nanomaterials in the Wet Processing of Textiles, 1: 113-134.

Wang, F., Tao, W. Y., Cheng, R. R., Wang, T., Gen, W. and Wen, F. 2005. Microstructure and properties of copper matrix composites reinforced by nano-SiC and nano-$Al_2O_3$ particles. Transactions of Nonferrous Metals Society of China, (S3): 136-139.

Wu, T. F., Qiu, Z. W., Lee, S. L., Lee, Z. G. and Lin, J. C. 2004. Effects of graphite on wear and corrosion behaviour of SiCp-reinforced copper matrix composites formed by hot pressing. Corrosion Engineering, Science and Technology, 39(3): 229-235.

Younis, S. B. 2011. Mechanical properties investigation of Cu–SiC composites using different percentage of Magnesium element. Journal of the College of Basic Education, 16(67).

Yusoff, M. and Hussain, Z. 2013. Effect of compaction pressure on Microstructure and properties of copper-based composite prepared by Mechanical alloying and powder metallurgy. In Advanced Materials Research. Trans Tech Publications, 795: 343-346.

Zeynelabdien, H. A., Mahmood, A. S. and Majeed, Z. N. 2021. Effect of addition of Tungsten Carbide on the structural and physical properties of an Aluminum-based system by powder method. In Journal of Physics: Conference Series. IOP Publishing, 99(1): 12-16.

Zhu, Q., Oganov, A. R. and Lyakhov, A. O. 2013. Novel stable compounds in the Mg–O system under high pressure. Physical Chemistry Chemical Physics, 15(20): 7696-7700.

**CURRICULUM VITAE**

## Personal Information

Name and Surname : Noor Jasim Zaboon AL-SAEDI

## Education

| | | |
|---|---|---|
| MSc | Çankırı Karatekin University<br>Graduate School of Natural and Applied Sciences<br>Department of Physics | 2020-Present |
| Undergraduate | Mustansiriyah University<br>College of Education<br>Department of Physics | 2002-2006 |